FOG

Freiberg Online Geoscience

FOG is an electronic journal registered under **ISSN 1434-7512**

2018, VOL 53

Benjamin Hildebrant

Characterizing the Reactivity of Commercial Steel Wool for Water Treatment

59 pages, 16 figures, 11 tables

Acknowledgements

I would like to thank my supervisor PD. Dr. Chicgoua Noubactep for giving me the opportunity to work with him and for his guidance and support along the way. I appreciate his patience and willingness to explain and demonstrate both theoretical and experimental aspects of the thesis work.

I would also like to thank PD. Dr. Tobias Licha for allowing me to use his laboratories and equipment during the experimental portion of the thesis work.

I am also very thankful for Arnauld I. Ndé-Tchoupé (University of Douala, Cameroon) for all of his support in providing samples, data, and guidance throughout the entire investigation.

Lastly I would like to express my gratitude to my family for all of their support for the last two and a half years. They have always encouraged me to dream big, and have made many sacrifices to help me pursue those dreams. Without their encouragement and support, this thesis would not have been possible.

Abstract

Metallic iron (Fe^0) has been used for water treatment systems since the 19^{th} century to remove a wide array of contaminants. Proper material selection and filter design are critically important for sustainable water treatment solutions. Fe^0-bearing materials cannot be properly characterized by physical parameters such as specific surface area or density, but rather must be characterized based on intrinsic reactivity assessed experimentally. Studies aiming at the characterization of the intrinsic reactivity of Fe^0-bearing steel wool (SW) were undertaken using a 2 mM ethylenediaminetetraacetate (Na_2-EDTA) solution in batch and column experiments. The dissolution kinetics of 15 SW specimens from various origins were investigated using modified protocols of the iron dissolution in EDTA test used in previous works to characterize the intrinsic reactivity of Fe^0 materials. Modifications to the protocol include: 1.) Decreasing/limiting the duration of the iron dissolution experiment, 2.) Increasing the volume of EDTA solution, and 3.) Increasing or decreasing the sample mass, depending on sample reactivity. The data was analyzed using the initial dissolution rate (k_{EDTA}). SW samples were able to be better characterized after modifications to the iron dissolution in EDTA test due to improved linearity of dissolution kinetics. Four of the SW samples (all of fine grade) SW 1, SW 5, SW 6 and SW 7 were selected and tested in extended iron dissolution in EDTA column experiments, along with granular iron (GI). Columns were filled with sand to a height of 10 cm, on top of which 0.50 g of SW or GI was placed. After columns were charged with a gravity fed 2 mM solution of EDTA, effluent samples from each column were taken and analysed for Fe concentration. After 53 leaching events, the results showed similar amounts of leached Fe from each of the columns containing SW and confirmed the observations of the batch tests that showed similar dissolution rates for the tested samples. The 15 SW specimens were additionally investigated for discoloration efficiency of methylene blue (MB) and Orange II in batch tests utilizing rotational shaking. All of the samples were more efficient at discoloration of anionic Orange II than cationic MB discoloration due to preferred adsorption of negatively charged Orange II onto positively charged in-situ generated iron hydr(oxides). Additionally, SW1, SW2, SW3, SW4, and SW6 were investigated for their capacity to remove fluoride in Fe^0 filters amended with sand. Effluent samples were analysed for fluoride and Fe concentration after each leaching event. The results show fluoride removal from all columns, but less than 20% on average for each column. SW appears to be a viable option for fluoride removal in use with household filters. Further research should be extended to include correlation of the intrinsic reactivity of SW specimens with their efficiency at removing different contaminants in water.

Table of Contents

List of Figures

List of Tables

List of Abbreviations

EDTA	**Ethylenediaminetetraacetic**
Fe^0/ZVI	**Metallic Iron/Zero Valent Iron**
Fe^{2+}	**Ferrous Iron**
Fe^{3+}	**Ferric Iron**
GI	**Granular Iron**
MB	**Methylene Blue**
SW	**Steel Wool**
TISAB	**Total Ionic Strength Adjustment Buffer**
WHO	**World Health Organization**

1. Introduction

1.1 Background

Most communities in the developed world have access to safe drinking water via a centralized water treatment plant. The same is true of large cities in developing countries. Yet in small rural or remote communities in developing countries no centralized water supply is available, likely due to the associated disadvantages, which include: 1.) high installation and maintenance costs, 2.) lack of steady power supply, 3.) lack of infrastructure, 4.) lack of technical knowledge to maintain infrastructure (Ndé-Tchoupé et al. 2015; Johnson et al. 2008a; Momba et al. 2009). Because of the lack of piped water in many poor villages and slums of developing countries, potentially polluted lakes, rivers, and shallow hand-dug wells become the main source of water (Johnson et al. 2008a). Decentralized water treatment systems have seen an increase in usage in the developing world. Not only does it offer a low cost, low energy, and low maintenance solution to treating contaminated water, it also allows small communities to customize their water treatment objectives based on local needs (Slaughter 2010; Sima and Elimelech 2013; Peter-Varbanets et al. 2012; Ndé-Tchoupé et al. 2015). Filtration systems using membrane technology are an ideal choice for some communities or households because of the lack of needed chemicals and the ability to produce high quality water while removing bacteria, viruses, and other microorganisms (Peter-Varbanets et al. 2012; Sima and Elimelech 2013; Ndé-Tchoupé et al. 2015). Yet gravity driven membrane filtration systems are not as effective for the treatment of water containing a high concentration of aqueous contaminant species, such as fluoride, nitrate, and arsenic. For this reason gravity fed filters using Fe^0 are becoming a popular choice for use with decentralized water treatment schemes in the developing world (Banerji and Chaudhari 2017; Gheju 2018; Heimann et al. 2018; Ndé-Tchoupé et al. 2018a; Ndé-Tchoupé et al. 2018b; Noubactep 2017, 2018). Not only are Fe^0-containing materials widely available throughout the world, but they have also been shown to remove a wide range of chemical (e.g. metalloids, nutients) and biological (e.g. bacteria, viruses) contaminants (Ngai et al. 2007; Gottinger, A, M. et al. 2013; Johnson et al. 2008a; Schäfer et al. 2007; Domga et al. 2015).

1.2 Fe^0 use in remediation and filters

Reynolds et al. (1990) are commonly reported to be the first to suggest that Fe^0 could be used in remediation work when they published their findings that galvanized steel and stainless steel used in groundwater monitoring devices were responsible for causing bias in the determination of halocarbons. Gillham and O'Hannesin (1994) used Fe^0 to accelerate the rate of degradation in 13 chlorinated methanes, ethanes, and ethenes, and suggested the use of Fe^0 in passive treatment systems. Years later they performed the first long term field test of Fe^0 for remediation purposes at Canadian Forces Base in Ontario, Canada by using a permeable barrier wall composed of granular iron and sand to remove trichloroethene and tetrachloroethene leaking from a contaminant source into the groundwater (Gillham and O'Hannesin 1998). Fe^0 in permeable reactive barriers has become a standard tool in environmental remediation practice (Gaun et al. 2015; Henderson and Demond 2007; Johnson et al. 2008b; Noubactep 2011, 2015).

Although water treatment with Fe^0 has gained much attention recently, it was already being applied to water filtration in Antwerp, Belgium as early as 1883 (Mwakabona et al. 2017). Fe^0 for use in household filters has been the subject of much research during the last two decades and is considered an adaptation of its use in permeable reactive barriers for remediation (Mwakabona et al. 2017; Gottinger, A, M. et al. 2013; Ngai et al. 2007; Gillham and O'Hannesin 1994, 1998; Henderson and Demond 2007; Comba et al. 2011). The first recent efforts of water treatment using Fe^0 amended filters focused on removing arsenic from natural waters in Southeast Asia and Latin America (Lackovic et al. 2000; Leupin and Hug 2005; Ngai et al. 2007; Hussam and Munir 2007; Noubactep et al. 2012b). Since then the science of Fe^0 filtration has been well established (Miyajima 2012; Caré et al. 2013; Domga et al. 2015; Phukam 2015, Ebelle et al. 2018) and Fe^0 filter designs have been researched and improved (Noubactep et al. 2009b; Noubactep 2010b, 2011, 2016, 2018b; Ndé-Tchoupé et al. 2015; Tepong-Tsinde et al. 2015; Naseri et al. 2017; Hildebrant and Ndé-Tchoupé 2018).

Fe^0 filters for water treatment are a viable option in developing countries in large part due to the low cost of Fe^0 materials. Fe^0 materials which have already been tested and shown effective for contaminant removal include iron fillings, iron nails, iron wire, scrap iron, sponge iron, and steel wool (Makota 2017; Naseri et al. 2017; Noubactep et al. 2009c). While few investigations so far have researched steel wool (SW) for removal of a wide range of contaminants, Tseng et al. (1984) used SW to generate iron oxides for the adsorption of ^{60}Co in order to facilitate the

environmental monitoring of a nuclear power plant. The study revealed that SW has potential as a source of Fe^0 for use in water filters (Ndé-Tchoupé et al. 2015). James et al. (1992) successfully used SW with sand and peat filters to remove phosphate from wastewater runoff and extend the service life of the filters, with Erickson et al. (2007) obtaining similar results with phosphate removal from storm water runoff. SW has also effectively been used to reduce the concentration of selenite in mine drainage (Ziyan et al. 2017).

1.3 Material characterization

Proper material selection and filter design are essential for sustainable water filters. SW and other Fe^0-bearing materials cannot be properly characterized by physical properties such as chemical composition, specific surface area, density, or size, but rather must be characterized by intrinsic reactivity which is calculated experimentally and not dependent on the system being investigated.

Early attempts to characterize the intrinsic reactivity of metals were carried out under experimental conditions that were very dissimilar to environmental conditions and made use of aggressive agents to attack the metallic surface (Evans 1939; Piwowarsky 1951). Additionally, these early methods could be expensive and considerably complicated (Noubactep et al. 2004).

Over the past 20 years, various investigations to characterize the intrinsic reactivity of Fe^0 materials have been undertaken (Westerhoff and James 2003; Noubactep et al. 2005; Reardon 1995, 2005; Li et al. 2016; Noubactep et al. 2009b; Birke et al. 2015; Naseri et al. 2017; Kim et al. 2014). The most affordable and simple methods were those of Noubactep and colleagues, who used the chelating agent ethylenediaminetetraacetic (EDTA) to initiate dissolution of Fe^0, and Reardon, who used the evolution of H_2 to characterize intrinsic reactivity (Reardon 1995; Noubactep et al. 2005; Naseri et al. 2017).

The present study uses SW as a source of Fe^0 for contaminant removal in use with sand amended filters. More specifically, this study presents a modified protocol of Noubactep et al. (2004) using iron dissolution in EDTA to characterize the intrinsic reactivity of SW, and uses the removal of a common groundwater contaminant species, fluoride, by SW to validate the effectiveness of the protocol.

1.4 Fluoride

Fluoride can be detected in all natural water sources at some concentration, while groundwater may contain elevated concentrations, depending on the local geology and amount of fluoride-bearing minerals present (Fawell et al. 2006). Common fluoride-bearing minerals include fluorite, apatite, rock phosphate, and topaz (Teotia et al. 1981). Dissolution of fluoride bearing minerals by water is the main source of fluoride in groundwater, although anthropogenic input such as pesticides, phosphate fertilizers, and industrial operations can result in high concentrations of fluoride in soil, which in turn may leach into groundwater (Kabata Pendias and Pendias 2001; Roy and Dass 2013; National Academy of Sciences 2006). While fluoride is often added in low concentrations to public water supplies (0.5-1.0 mg/L) as protection against dental caries, the WHO sets a recommended maximum fluoride concentration of 1.5 mg/L for safe drinking water. Intake of water containing higher concentrations of fluoride over a long time period can lead to dental and skeletal fluorosis (WHO 2017). Dental fluorosis symptoms include mottling and browning of the teeth, with some severe cases leading to tooth loss and pus seepage from the gums. Skeletal fluorosis symptoms include stiffened limbs and vertebral columns, joint pain, difficulty walking, and weakened bones that fracture easily. In severe cases skeletal fluorosis can be crippling (Bharati et al. 2005). India, China, Central and East Africa, and parts of South America have high concentrations of fluoride in groundwater and surface water, yet local areas of high fluoride concentration can be found in most parts of the world (WHO 2017; Nair et al. 1984).

1.5 Thesis objective

Recent investigations have shown that Fe^0 bearing steel wool (SW) has potential for facilitating the removal of contaminants in use with household filters for decentralized safe drinking water provision, with the added benefit that SW is one of the most widely available and affordable sources of Fe^0 (Naseri et al. 2017; Ndé-Tchoupé et al. 2015). Despite decades of research on the suitability of Fe^0 materials for environmental remediation, very little focus has been put on the screening of SW or other Fe^0 sources based on their intrinsic reactivity (Noubactep et al. 2004; Ndé-Tchoupé et al. 2015; Noubactep et al. 2005; Reardon 1995; Westerhoff and James 2003; Hildebrant and Ndé-Tchoupé 2018). Without a standard protocol to test for intrinsic reactivity, the selection of Fe^0 materials for field use is done at random, which leads to discrepancies in results and difficulties in comparing results from different sources. The objective of this thesis is

to establish a standard protocol for the characterization of the intrinsic reactivity of steel wool (SW). The protocol of Noubactep et al. (2004; 2005) for the characterization of Fe^0 materials using iron dissolution in 2 mM ethylenediaminetetraacetic (EDTA) solution is the basis of the new protocol in the present work, with modifications made to account for the highly reactive nature of steel wool.

1.6 Thesis outline

The present work contains five chapters and an appendix containing relevant experimental data. After a presentation of background information in chapter 1, chapter 2 gives an overview of processes involved in the iron corrosion and contaminant removal processes. Chapter 3 describes the materials and methods used to carry out the investigations, and chapter 4 is a presentation and discussion of the results of these investigations. Chapter 5 provides an overview of the experimental results and their significance, as well as suggests further areas of research to be investigated as a continuation of the present study. The appendix provides experimental data as recorded during the experimental phase.

2. Theoretical background: Oxidative iron dissolution

2.1 Aqueous iron corrosion

Oxidative iron dissolution, or iron corrosion, is the process by which Fe^0 loses electrons to become Fe^{2+} after the parent Fe^0 is immersed in an aqueous solution. This process can be considered as an electrochemical process because electrons are released from Fe^0 in an anodic site and migrate to a cathodic site, where they are utilized in other chemical reactions. Because Fe^0 essentially acts as an electrode, using Fe^0 to produce in-situ generated iron oxides for contaminant removal can be considered similar to the process of contaminant removal by electro-coagulation (Noubactep et al. 2009c; Tepong-Tsinde et al. 2015).

Films of iron oxide corrosion products form around the Fe^0 material, which slows down the iron dissolution rate over time. Because the films are porous, dissolved oxygen and other oxidizing agents are able to permeate through the matrix of the oxidative film as well as causing the iron oxide to precipitate and expose a fresh Fe^0 surface, allowing oxidative iron dissolution to continue (Dickerson et al. 1979). Some of the main corrosion products of metallic iron include Magnetite (Fe_3O_4), Hematite (α-Fe_2O_3), Maghemite (γ-Fe_2O_3), Geothite (α-FeOOH), Akageneite (β-FeOOH), Lepidocrocite (γ-FeOOH), Ferrous Hydroxide ($Fe(OH)_2$), and Ferric Hydroxide ($Fe(OH)_3$) (Noubactep 2010d).

Iron corrosion plays an important role in contaminant removal because the corrosion products have sponge-like matrixes that can effectively entrap a wide array of contaminants which may then be later chemically altered through reduction or oxidation (Noubactep 2010d, 2010a; Ghauch et al. 2010; Stratmann and Müller 1994). Noubactep (2011) describes the entire iron corrosion process for a single Fe^0 atom (soluble species) as:

$$Fe^0 \rightarrow Fe^{2+}/Fe^{3+}(H_2O)_6 \rightarrow Fe^{2+}/Fe^{3+}(OH)_n \rightarrow FeOOH \rightarrow Fe_2O_3 \rightarrow Fe_3O_4 \qquad \text{(eq. 1)}$$

For insoluble species the iron corrosion process can be described as:

$$Fe^0 \rightarrow Fe(OH)_2 \,/\, Fe(OH)_3 \rightarrow FeOOH \rightarrow Fe_2O_3 \rightarrow Fe_3O_4 \qquad \text{(eq. 2)}$$

Fe^0 dissolution can be considered as an anodic reaction in which electrons are donated:

$$Fe^0 \leftrightarrow Fe^{2+} + e^- \qquad \text{(eq. 3)}$$

Important reactions occurring at cathodic sites on the Fe^0 surface include reduction of oxygen and hydrogen:

$$O_2 + 4e^- + 2H_2O \leftrightarrow 4OH^- \quad \text{(eq. 4)}$$

$$2H^+ + 2e^- \leftrightarrow H_2 \quad \text{(eq. 5)}$$

Fe^{2+} produced in equation 3 may be deposited as part of an oxide film or it may be dissolved into the solution and further oxidized to Fe^{3+}, which in turn can react with Fe^0:

$$Fe^{2+} \leftrightarrow Fe^{3+} + e^- \quad \text{(eq. 6)}$$

$$Fe^0 + 2Fe^{3+} \leftrightarrow 3Fe^{2+} \quad \text{(eq. 7)}$$

Fe^{2+} and Fe^{3+} ions react with water to form hydroxides which polymerize to induce crystallization and precipitation of Fe^{2+}/Fe^{3+} oxides/hydroxides:

$$Fe^{2+} + 2H_2O \leftrightarrow Fe(OH)_2 + 2H^+ \quad \text{(eq. 8)}$$

$$Fe^{3+} + 3H_2O \leftrightarrow Fe(OH)_3 + 3H^+ \quad \text{(eq. 9)}$$

$$Fe(OH)_2 \leftrightarrow FeO + H_2O \quad \text{(eq. 10)}$$

$$Fe(OH)_3 \leftrightarrow FeO(OH) + H_2O \quad \text{(eq. 11)}$$

$$2FeO(OH) \leftrightarrow Fe_2O_3 + H_2O \quad \text{(eq. 12)}$$

$$3Fe_2O_3 + H_2 \leftrightarrow 2Fe_3O_4 + H_2O \quad \text{(eq. 13)}$$

Throughout the process of iron oxidation, a cycle of expansion and contraction is undergone by the surface area of Fe materials. In addition to the previously mentioned equations describing the iron corrosion process, Noubactep (2011) characterized the iron corrosion process using the following equation that includes the coefficient of volumetric expansion (V_{oxide}/ V_{Fe}) from Caré et al. 2008:

$$Fe^0\ (1) \rightarrow Fe_2(HO)_6\ (6.4) \rightarrow FeOOH\ (3.0) \rightarrow Fe_2O_3\ (2.2) \rightarrow Fe_3O_4\ (2.1) \quad \text{(eq. 14)}$$

From the given ratios, it can be seen that dissolved Fe undergoes an expansion and then a contraction. But in comparison to the starting Fe^0 material, the end products have a higher coefficient of volumetric expansion, demonstrating that the overall effect is expansion, which can lead to clogging/passivation of a poorly designed filter (Noubactep 2011).

The iron corrosion process leads to layers of corrosion products being deposited, also known as oxide films. These oxide films have four distinctive layers: 1) a corroded floor, 2.) a porous core containing both fluids and solids, 3.) a comparatively dense shell-like layer surrounding the fluid/solid-containing core that provides stability to the scale, and 4.) a surface layer that is at the scale-water interface and is loosely connected to the shell-like layer (figure 1) (Sarin et al. 2004b). The corroded floor is essentially the corroded metal surface that is acting as a source of iron for the corrosion products of the outer layers. The porous core contains high concentrations of Fe(II) in the form of solids such as $Fe(OH)_2$, Fe_3O_4, and $FeCO_3$, as well as dissolved in the aqueous solution filling the cavity pore spaces (Sarin et al. 2001). The dense shell-like layer surrounding the porous core consists mostly of Fe_3O_4 and α-FeOOH and acts to separate the surrounding aqueous solution and the Fe(II) of the core, which can be easily oxidized (Sarin et al. 2001; Sarin et al. 2004b). The top surface layer of loosely held iron oxide phases, such as $Fe(OH)_3$, can easily be swept away and transported into the surrounding aqueous solution, especially when hydraulic surges or fluxes occur. Transportation of these particles into solution can cause turbidity and discoloration of the solution (Sarin et al. 2004b).

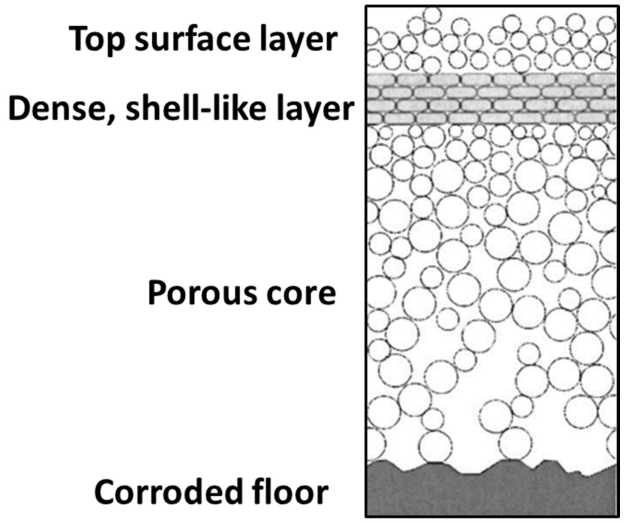

Figure 1. Model of the layers of an iron oxide film, as presented by Sarin et al. (2004b).

In addition to high flow rates, other factors can affect the kinetics of iron dissolution. Water quality parameters such as dissolved oxygen (DO) and pH play important roles as well. Sarin et al. (2004a) demonstrated that an increase in DO concentration results in a decrease in iron release and causes precipitation. High flow rates speed up the transport of DO to the surface of the oxide film, whereby Fe^{2+} is oxidized to the less soluble Fe^{3+} which is then precipitated within the oxide film, effectively increasing the rate of corrosion. This leads to a denser and less permeable oxide film that inhibits the diffusion of Fe^{2+} to the bulk solution.

When water pH is greater than 10, the rate of corrosion decreases as pH increases. This occurs because DO reacts increasingly more with $Fe(OH)_2$ in the oxide film, leading to the formation of Fe_2O_3, which is not easily dissolved. Between pH values 4-10 the rate of corrosion is mostly determined by the rate at which DO reacts with atomic hydrogen, leading to the depolarization of the Fe^0 surface and the continuation of reduction reactions. At pH values lower than 4 the iron corrosion rate increases due to the solubility of FeO, which is dissolved instead of forming an oxide film on the Fe^0 surface. Therefore the Fe^0 surface is exposed to the acidic bulk solution, leading to an increased rate of corrosion (DOE 1993).

2.2 Mass transport

Fe(II) ions generated near the surface of the source of Fe^0 are moved toward the bulk aqueous solution in a flux, while oxidants such as dissolved oxygen migrate from the bulk aqueous solution towards the Fe^0 surface, allowing the corrosion process to continue (Sarin et al. 2004b). This process is known as mass transport. Under environmental conditions, diffusion and advection are the main types of mass transport. Diffusion is the movement of molecules or ions due to concentration gradients (Zeeck et al. 2003), and advection is the movement of molecules or ions with the flow of a transport medium (Hilberg 2015). Advection is the main mass transport process occurring at the surface layer of the oxide film at the water-oxide film interface. Near the surface of Fe^0 within the porous core, diffusion is the main transport mechanism due to the lack of turbidity within the shell-like layer of corrosion products (Sarin et al. 2004b; Miyajima 2012; Noubactep 2009a). Concentration gradients of dissolved species on

both sides of the oxide film lead to diffusion of these species towards or away from the surface of the Fe^0 material (Gunawardana et al. 2011), and the oxide film is essentially an electron conductor that allows the transfer of electrons from the Fe^0 surface to the bulk aqueous solution, as well as contaminants across the oxide film (Scherer et al. 2000; Phukam 2015, Alyoussef 2018). In non-disturbed batch and column experiments, diffusion is the mechanism by which molecules come into contact with Fe^0 and associated corrosion products. Experiments performed under disturbed conditions, such as rotational shaking, rely on advection as the primary mass transport mechanism (Noubactep et al. 2009a).

2.3 Contaminant removal mechanisms

Early research on Fe^0 technology focused on reductive transformation as the main mechanism of contaminant removal as electron transfer from the metal body to the contaminant can potentially lead to direct or indirect reduction of the contaminant, with Fe^0 being oxidized (Matheson und Tratnyek 1994; Weber 1996; Gillham and O'Hannesin 1998). Yet considering the wide range of both reducible and non-reducible species, including viruses and bacteria, that have successfully been removed from water using Fe^0 (Hussam and Munir 2007; Henderson and Demond 2007; Bojic et al. 2001; Bojic et al. 2004; You et al. 2005), it is apparent that other mechanisms are responsible for contaminant removal (Noubactep 2010c). The fundamental mechanisms of contaminant removal in the Fe^0/ H_2O systems include (i) adsorption, (ii) co-precipitation, and (iii) adsorptive size exclusion (Ghauch et al. 2011; Gheju and Balcu 2011; Noubactep 2007, 2008, 2011, 2018c). Direct or indirect reduction of contaminants could occur in conjunction with these mechanisms, but the present work will focus on these main mechanisms rather than on contaminant reduction.

2.3.1 Adsorption

Adsorption is the process by which an adsorbate such as molecules, ions, or atoms are attracted to and accumulate on an adsorbent, or surface. Adsorption can take place at any interface such as liquid-liquid, liquid-solid, gas-liquid, or gas-solid interfaces, yet the liquid-solid interface is the most important interface in Fe^0-H_2O water remediation (Vasireddy 2005). Adsorption can occur as physical adsorption, in which electrostatic and Van der Waal forces are responsible for bonds between adsorbent and adsorbate, and chemical adsorption, in which stronger covalent bonds are formed (Ghosemi and Asadpour 2007). Many factors such as physical, chemical, and structural

characteristics of both the adsorbent and the adsorbate, as well as specific surface area of the adsorbent, can affect total adsorption capacity (Ghosemi and Asadpour 2007; Smith and Coakley 1983).

2.3.2 Co-precipitation

Co-precipitation occurs when a contaminant is sequestered from solution by a precipitating phase, such as iron oxides and hydroxides (corrosion products), which leads to settling of the targeted contaminant. Co-precipitation can effectively remove many types of contaminants regardless of whether the contaminant is ionic, organic or inorganic, bacteria, or even a virus (Crawford et al. 1993; Diao and Yao 2009; You et al. 2005; Hussam and Munir 2007). Co-precipitation includes three types of processes (Crawford et al. 1993; Karthikeyan et al. 1997) by which contaminants can be effectively removed from solution:

1.) Surface absorption occurs when the contaminant is adsorbed onto the surface of hydrous ferrous oxides.
2.) Mixed crystal formation occurs when a solid is formed by incorporating the contaminant into the lattice of hydrous ferrous oxides.
3.) Mechanical entrapment occurs when the precipitate encloses the contaminated solution as it is formed.

Direct or indirect reduction of contaminants entrapped within the precipitate can then occur after co-precipitation. In the case of species that aren't reduced, the contaminant is nonetheless captured within the iron-oxide matrix and therefore effectively removed from solution, making co-precipitation more effective than just adsorption alone (Crawford et al. 1993). Contaminants that are co-precipitated with an iron-oxide will not be released into the environment as long as the iron-oxide is not dissolved (Noubactep 2009a, 2010a; Ghauch et al. 2010; Ghauch et al. 2011).

2.3.3 Adsorptive size exclusion

Adsorptive size exclusion, also known as straining, is the contaminant removal mechanism in which particles of the targeted contaminant that are larger than the void space of the filter cannot pass through the void space and are essentially trapped. A "cake layer" forms as the concentration of trapped contaminants increases and forms a layer over the filter medium pores,

which in turn can facilitate the filtering of increasingly smaller contaminant particles (Holdrich 2002; USAPHC 2011).

2.4 Iron dissolution in EDTA

Over the past 20 years, various investigations to characterize the intrinsic reactivity of Fe^0 materials have been undertaken (Westerhoff and James 2003; Noubactep et al. 2005; Reardon 1995, 2005; Li et al. 2016; Noubactep et al. 2009b; Birke et al. 2015; Naseri et al. 2017). The most affordable and simple methods were those of Noubactep, who used the chelating agent ethylenediaminetetraacetic (EDTA) to initiate dissolution of Fe^0, and Reardon, who used the evolution of H_2 to characterize intrinsic reactivity (Reardon 1995; Noubactep et al. 2005; Naseri et al. 2017).

At neutral pH metallic ions are strongly complexed by EDTA (eq. 15 and 16). This procedure has been used to study the remobilization of metals from iron and manganese oxides (Nowak et al. 1996). Metal oxide dissolution by chelating agents like EDTA releases metal ions back into solution (Noubactep et al. 2004). Therefore avoiding metal oxide formation and accelerating the corrosion process are two advantages of this process.

$$Fe^{2+} + EDTA = FeEDTA^{2+} \quad \text{(eq. 15)}$$

$$Fe^{3+} + EDTA = FeEDTA^{3+} \quad \text{(eq. 16)}$$

Noubactep (2009b; Noubactep et al. 2009b) introduced the parameter $k_{EDTA,}$ with the goal of enabling purposeful selection of Fe^0 material. K_{EDTA} is the slope of the line of oxidative dissolution of ions of a Fe^0 material as a function of time, and is determined in batch experiments using a 2 mM EDTA solution. This method yields the intrinsic reactivity of a material under the given experimental conditions (Noubactep et al. 2009c).

Btatkeu-K et al. (2013b) used the EDTA method to closely correlate k_{EDTA} value to the discoloration of methylene blue in column studies. Therefore the comparison of k_{EDTA} values has been proposed as a tool to characterize the intrinsic reactivity of Fe^0 and facilitate the discussion of results from different sources (Naseri et al. 2017).

The investigation described in this thesis uses EDTA to initiate iron dissolution of samples of steel wool. This method has been used in other studies to investigate the iron dissolution of samples of scrap metal, granular iron, cast iron, carbon steel, and commercially available Fe^0

materials (Noubactep et al. 2005; Noubactep et al. 2004). Difficulties in characterizing the intrinsic reactivity of Fe^0 arises primarily from two parameters: (i) the formation of oxide layers on Fe^0, and (ii) the interactions of dissolved species within the oxide layers on Fe^0 (Noubactep 2010a). The EDTA method is particularly useful for characterizing Fe^0 materials because it prevents the formation of an oxide layer on the surface of the tested material (Sikora und Macdonald 2000; Pierce et al. 2007; Noubactep 2009b; Noubactep et al. 2005).

It is expected that the total aqueous iron concentration ($[Fe]_t$) (Equation 15) will be a linear function of time (Equation 16) at any time (t) after the start of the experiment (t_0).

$$[Fe]_t = [Fe^{2+}] + [Fe^{3+}] + [FeEDTA^{2+}] + [FeEDTA^{3+}] \quad \text{(eq. 17)}$$

$$[Fe]_t = at + b \quad \text{(eq. 18)}$$

Replacing a with k_{EDTA}, we get

$$[Fe]_t = (k_{EDTA})t + b \quad \text{(eq. 19)}$$

Ideally, under given experimental conditions, SW concentration should increase continuously with time from 0 mg L^{-1} at the start of the experiment ($t_0 = 0$) to 112 mg L^{-1} (2 mM) at saturation when a 1:1 complexation of Fe and EDTA occurs. The individual Fe^0 samples can be described by the regression parameters k_{EDTA} and b. The calculated intercept b refers to the iron concentration at t_0 (ideally zero) and gives an estimation of the amount of corrosion products on the Fe^0 sample (Noubactep et al. 2005). Therefore,

$$b = [Fe]_{t0}$$

and,

$$[Fe]_t = (k_{EDTA})t + [Fe]_{t0} \quad \text{(eq. 20)}$$

2.5 Design of Fe^0 amended sand filters

Filter systems for water treatment using Fe^0 as the source of corrosion products are at risk of clogging and losing their functionality and effectiveness at removing contaminants. Possible mechanisms of filter clogging include: 1.) adsorption of fouling materials, 2.) bio-corrosion, 3.) cake formation, and 4.) volumetric expansion of iron (Noubactep 2010b; Miyajima 2012; Noubactep et al. 2010). Most filter clogging can be attributed to the volumetric expansion of iron, especially in water with pH > 4. Adding a chemically inert material like sand can prolong

filter lifespan by increasing void space between particles and providing ample volume for corrosive iron expansion (Caré et al. 2008; Noubactep 2011; Noubactep and Caré 2013). Sand does not cause porosity loss in filters because sand, unlike iron, has no expansive properties.

The reactive zone of a Fe^0/sand filter is where iron (hydr)oxides are generated for subsequent contaminant removal in the filter. While the Fe^0 material is a necessary part of an effective filter, it is not beneficial to design a filter using 100% Fe^0 without an inert material. A filter consisting of only Fe^0 material will eventually lose porosity due to the expansive nature of the iron corrosion process and be rendered useless for water filtration (Btatkeu-K et al. 2014; Gheju and Balcu 2019; Hussam 2009; Hussam and Munir 2007; Noubactep et al. 2010). Based on the results of modeling clogging in Fe^0/quartz systems (Noubactep et al. 2010), it has been suggested that the volumetric proportion of Fe^0 should not exceed 51%, otherwise the filter will lose permeability before all of the Fe^0 can be exhausted, leading to material wastage (Noubactep et al. 2010; Btatkeu-K et al. 2014; Noubactep et al. 2012a). Filters using 25% Fe^0 have been shown to be the most sustainable design (Miyajima 2012; Tepong-Tsinde et al. 2015; Ndé-Tchoupé et al. 2015). In order to insure that sufficient void space is available for the process of iron corrosion expansion, filters using a reactive zone sandwiched between two layers of inert sand offers a simple yet effective design for Fe^0 filters amended with sand (Phukam 2015; Miyajima 2012; Btatkeu-K et al. 2014).

3. Materials and Methods

3.1 Aqueous Solutions

3.1.1. EDTA

The ethylenediaminetetraacetic acid (EDTA) solution used for the experiments was prepared by dissolving an analytical grade disodium salt of EDTA (Na_2-EDTA) in tap water and diluting to a concentration of 0.002M (2mM). The used Na_2-EDTA salt from Merck has a given molar weight of 336.28 g/mol.

3.1.2 TISAB

Total ionic strength adjustment buffer (TISAB) was used to regulate the ionic strength and pH of samples prior to determination of fluoride concentration with the ion selective electrode. The buffer solution was prepared by adding 1500 mL of tap water to a 2500 mL glass beaker, to which 114.0 mL of glacial acetic acid, 116.0 g of table salt (NaCl), and 6.42 g of Na_2-EDTA were added. The mixture was heated and stirred with a magnetic stir rod and then allowed to cool to room temperature. Additional tap water was then added until the total solution volume reached 2000 mL, and the pH was adjusted by using a 5 M NaOH solution until a pH value of 5.3 was obtained. The TISAB solution was stored in clean polyethylene bottles.

3.1.3 Methylene Blue ($C_{16}H_{18}ClN_3S$)

Analytical grade Methylene Blue was purchased from Merk Acros Organics and used as received. The working solution had a concentration of 10.0 mg/L. MB is a cationic dye that has a strong affinity for the surface of negatively charged solids (Imamura et al. 2002). The dye changes from green to dark blue after being oxidized, and changes from dark blue to colorless after being reduced (Phukam 2015). MB has a maximum light absorption wavelength of 664.5 nm and a molecular mass of 319.85 g/mol.

3.1.4 Orange II ($C_{16}H_{11}N_2NaO_4S$)

Analytical grade Orange II dye was purchased from Sigma Aldrich and used as received. The working solution had a concentration of 10.0 mg/L. Depending on the pH of the medium, Orange II can exist in three different forms in aqueous solution because it has two pKa values (10.6 and

1.0) (Abramiam and El-Rassy 2009). It is an anionic azo dye that is strongly attracted to the surfaces of cationic materials. Orange II has a maximum light absorption wavelength of 485 nm and a molecular mass of 350.32 g/mol (Asgari et al. 2013).

3.1.5 Additional solutions

A standard iron solution (1000 mg L^{-1}) from Baker JT® was used to calibrate the spectrophotometer. In preparation for spectrophotometric analysis ascorbic acid was used to reduce Fe^{III}-EDTA in solution to Fe^{II}-EDTA. 1,10 orthophenanthroline (ACROS Organics) was used as reagent for Fe^{II} complexation prior to spectrophotometric determination. Other chemicals used in this study included L(+)-ascorbic acid, L-ascorbic acid sodium salt, and sodium acetate. All chemicals were of analytical grade.

3.2 Solid Materials

3.2.1 Sand

The sand used in all of the column experiments is commercially available for aviculture (‘‘Aquarienkies” sand from Quarzverpackungwerek Rosnerski Königslutter/Germany) The grain sizes of used Aquarienkies sand ranged between 2.0 and 4.0 mm (average diameter). The sand was used without additional pre-treatment or characterization. Sand was used because of its worldwide availability and its use as admixing agent in Fe^0/H_2O systems (Trois and Cibati 2015).

3.2.2 Steel Wool (Fe^0)

A total of fifteen different types of steel wool were used in this work. Six varieties of SW were purchased at a local hardware store in Göttingen and two steel wool varieties were purchased in Arusha (Tanzania). Four of the steel wool samples from Germany were from the trademark brand RASKO, consisting of grades 00, 0, 1, 2. The other two German steel wool varieties were a stainless steel Topfreiniger and a variety from the trademark brand Bobby Mat. The Bobby Mat variety was a fine grade, while the grade of the stainless steel Topfreiniger was not specified, but is herein classified as coarse grade. The two steel wool varieties purchased in Arusha (produced in Kenya) included Champion and Sokoni trademark brands, both being of a fine grade. Five of the steel wools were purchased in Douala (Cameroon): Trademark brand Grand Menage extra fine and fine steel wools, trademark brand Socapine very fine steel wool, Magic Mamy

trademark brand coarse steel wool, and a generic coarse steel wool. An additional two specimens were produced in China: Trademark brands Suprawisch fine grade steel wool and Lijia medium grade steel wool. The specifications of the steel wool specimens can be seen below in table 1. No information about manufacturing processes (e.g., raw material, heat treatment) was available to assist with subsequent data interpretation. It is well reported that the specific surface area (SSA) of iron materials is one of the predominant factors in controlling reactivity and is directly related to the material size (Johnson et al. 1996; Ponder et al. 2000; Liou et al. 2005). The materials investigated in this study have a variety of different grades with resultant differences in specific surface area, although exact values were not available or determined. However, it was not the objective of this study to investigate the impact of the specific surface area on the reactivity of these different materials, but rather to compare the reactivity of the materials in their typical state in which they might be used for field applications. Apart from chopping the SW samples into pieces of 1-2 mm in length, all materials were used for experiment in an 'as received' state.

Table 1. Overview of the fifteen different steel wool (SW) specimens used in these experiments. The SW vary from extra fine to coarse grade, and come from Germany, Kenya, Cameroon, and China. Information about exact thickness was only available for the specimens from China and Cameroon.

Material Code	Size	Grade	Thickness (µm)	Trade name
SW1	fine	00	n.a.	RASKO (Germany)
SW2	medium	0	n.a.	RASKO (Germany)
SW3	medium	1	n.a.	RASKO (Germany)
SW4	medium	2	n.a.	RASKO (Germany)
SW5	fine	00	n.a.	Champion (Kenya)
SW6	fine	00	n.a.	SOKONI (Kenya)
SW7	fine	00	n.a.	BOBBY MAT (Germany)
SW8	coarse	2	n.a.	Stainless steel Topfreiniger (Germany)
SW9	fine	00	40	SOCAPINE (Cameroon)
SW10	extra fine	000	35	Grand Menage (Cameroon)
SW11	fine	0	50	Stainless steel SUPRAWISCH (China)
SW12	medium	1	60	LIJIA (China)
SW13	fine	0	50	Grand Menage (Cameroon)
SW14	coarse	2	75	MAGIC MAMY (Cameroon)

SW15	coarse	3	90	Generic steel wool (Cameroon)

3.3 Experimental Procedure

3.3.1 Iron dissolution in EDTA

3.3.1.1 Batch experiments

Four different batch experiments were conducted at room temperature (22 ± 2 ^{0}C) using the following procedure. During this time the beakers were left undisturbed in the laboratory, and out of direct sunlight in order to limit Fe^{III} photo-degradation (Arai et al. 2008).

Experiment 1: A 0.1g sample of each of the steel wools (SW1-SW8) was weighed and placed in a 70 mL beaker with 50 mL of 2mM EDTA solution (2 g/L SW). Samples from each of the beakers were taken over a 72 hour time period (3 days).

Experiment 2: A 0.01g sample of each of the used steel wools (SW1-SW8) was weighed and placed in a 70 mL beaker with 50 mL of 2mM EDTA solution. Samples of the solutions were taken over a 100 hour time period.

Experiment 3: For the third experiment, three separate batch experiments were conducted simultaneously during a 24 hour time period, with the objective of achieving better linearity of oxidative Fe dissolution and thus more conclusive parameters of dissolution efficiency. The simultaneously run experiments were set up as follows:

3a: A 0.01g sample of each of the steel wools used (SW1-SW8) was weighed out and placed in 50 mL of 2mM EDTA solution, just as in batch experiment 2 as described above.

3b: In this batch experiment, the volume of EDTA solution was doubled. A 0.01 g sample of each steel wool specimen (SW1-SW8) was weighed out and placed in 100 mL of 2mM EDTA solution.

3c: A 0.01 g sample of each steel wool (SW9-SW15), along with a sample of granular iron, were weighed out and placed in 50 mL of 2mM EDTA solution.

At intervals of increasing time difference, 1 mL samples were taken from each of the beakers containing steel wool (and granular iron) samples in EDTA solution. This procedure was carried out over a 24 hour time period.

Experiment 4: The final Fe dissolution batch experiment was performed using triplicates of each of the following samples placed in beakers containing 50 mL of 2mM EDTA solution: 0.01 g samples of SW1, SW5, SW9, and granular iron, in addition to a 0.1 g sample of granular iron. The values presented in the results for each sample investigated are the average value of the corresponding triplicates.

3.3.1.2. Column experiment

Five glass columns were filled with 10 cm of sand, on top of which 0.500 grams of Fe^0 material was placed. Each column contained one of the five types of Fe^0 materials being tested. Four steel wool specimens (SW1, SW5, SW6, SW7) and granular iron (GI) were chosen to use in the column experiment. The columns were then intermittently charged with a gravity driven 2 mM EDTA solution and allowed to set for at least 24 hours.

The EDTA solution from each column was then drained and collected in a glass cylinder 3-5 times per week. The collected volume was measured and recorded for each leaching event. 0.5 to 2.0 mL of the effluent solution was taken, extended to 10 mL and used for the determination of iron concentration. After each column was drained of EDTA solution and the previously mentioned steps carried out, each column was refilled with newly prepared EDTA solution and the procedure was repeated. The experiment was performed at room temperature (22 ± 2 °C).

3.3.2 Dye discoloration

Rotational shaking facilitates the adsorption and co-precipitation of contaminants, leading to a faster transportation time from the aqueous phase to the surface of Fe^0 materials (Noubactep et al. 2009a). Two different batch experiments were set up in order to investigate the effect of Fe^0 on different contaminants. The first dye batch experiment involved two sets of Fe^0 materials, with each set containing 10 different samples of triplicates, for a total of 30 samples per set. Three 0.05 g samples of each of the steel wool specimens (SW1-SW8), as well 3 samples of granular iron were weighed out for each batch set. 3 blanks containing no source of Fe^0 were used in each set as a reference. The samples were placed in test tubes and then each set was filled with either Orange II or MB, with each dye at a concentration of 10 mg/L. 22 mL was added to

each test tube. The two batch sets were then left under shaken conditions at 75 rotations per minute (rpm) for 8 weeks. At the end of 8 weeks, the samples were analyzed for dye concentration. Dye concentration was determined using the Cary 50 Varian UV-Vis Spectrophotometer.

This same experiment was repeated for a shorter 2 week time period using SW1- SW12 and granular iron, with a triplicate set containing no source of Fe^0 to be used as a reference. Triplicates of each Fe^0 specimen were used for both Orange II and MB, for a total of 84 samples. The average value of each triplicate was determined and used for the results.

3.3.3 Application: Fluoride removal

Five glass columns were filled with multiple layers of sand and sand/steel wool mixtures. 200 mL of sand was poured into the bottom of each column. To assure that the sand was optimally compacted the columns were gently tapped with a 100 mL PET flacon containing water. The reactive zone was placed on top of the sand layer. This reactive zone consisted of a total of 2 grams of steel wool mixed with 100 mL of sand. The investigated steel wool specimens were SW1, SW2, SW3, SW4, and SW6 (table 2). The steel wool was cut into small pieces (1-2cm) so that layers of sand could be interspersed between layers of steel wool. On top of the reactive layer, an additional 100 mL of sand was added.

Table 2. Selected steel wool specimens for investigation in column studies with 25 mg/L fluoride solution. 2.0 g of each sample was cut into small pieces and placed in the reactive zone of its respective column.

	Column 1	Column 2	Column 3	Column 4	Column 5
Steel Wool	SW 1	SW 2	SW 3	SW 4	SW 6
Mass (g)	1.985	1.989	2.006	2.009	1.996

The columns were then charged with a gravity driven water solution containing 25mg/L of fluoride. 15 mL of effluent from each column was collected in plastic sampling containers, after the fluoride solution had been in contact with the steel wool and sand filter for at least 24 hours. These effluent samples were used to determine the fluoride concentration, therefore only plastic containers, not glass, could be used. The attraction of a negatively charged fluoride atom to positively charged glass could have resulted in a reading for fluoride concentration that is lower

than the actual concentration in the sample. An additional 10 mL water sample from each column was collected in a glass test tube in order to determine iron concentration. Unlike fluoride, the iron ions are positively charged and therefore will not be attracted to the positively charged glass surface of the test tube. Addition samples from each column were taken for pH determination. The volume of effluent collected from each column was recorded for every sampling event. Each time after samples were taken for iron, fluoride, and pH determination, the columns were refilled with freshly prepared fluoride solution.

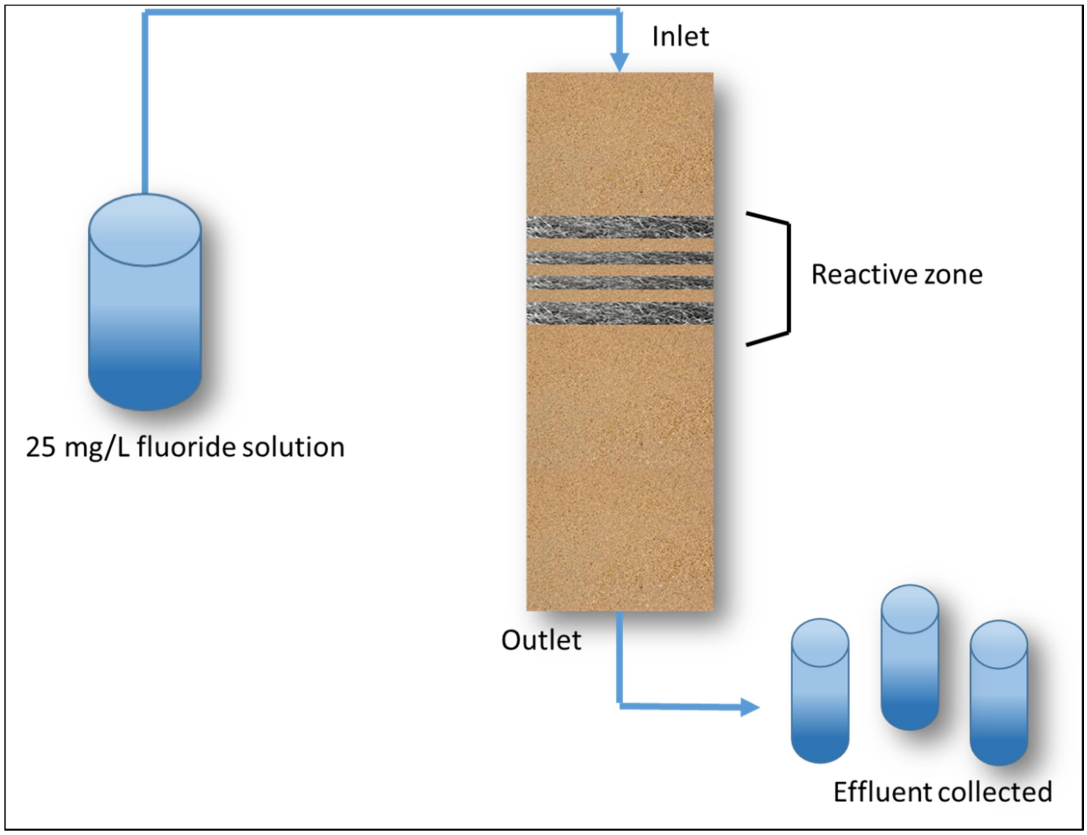

Figure 2. Graphic representation of the experimental set up of the fluoride removal experiment.

3.4 Analytical Methods

3.4.1 UV-Vis Spectra method

A Cary 50 Varian UV-Vis Spectrophotometer was used to determine dye and total dissolved iron concentration of the samples. The wavelength was set to a wavelength of 510 nm, 664.5 nm, and 485.0 nm for dissolved iron, MB, and Orange II concentration, respectively. Determination of

dissolved iron followed the 1,10 orthopenanthrolene method (Saywell and Cunningham 1937). Iron samples were prepared by combining:

10 mL of sample + 1 mL ascorbic acid + 8 mL H_2O + 1 mL 1,10-ortho-phenanthroline

The test tubes containing the prepared samples were then shaken to ensure proper mixing and allowed to set on the work bench 10-15 minutes before iron determination with the UV-Vis Spectrophotometer.

Dissolved iron, MB, and Orange II were calibrated using standard solutions of known concentration. For iron determination, standard solutions of 0, 2, 4, 6, 8, and 10 mg/L were prepared from an iron stock solution and tap water (table 3). Calibration for the dyes was performed by using standard dye solutions of 0, 2.5, 5.0, 7.5, and 10 mg/L for both MB and Orange II.

Table 3. Six standard iron solutions were used for the calibration of the Spectrophotometer before determination of iron in collected samples.

Standard	[Fe]	V_0	V_{H2O}
		(mL)	(mL)
1	0,00	0,00	10,00
2	2,00	2,00	8,00
3	4,00	4,00	6,00
4	6,00	6,00	4,00
5	8,00	8,00	2,00
6	10,00	10,00	0,00

3.4.2 pH meter

The pH value of samples were measured with combined gas electrodes (WTW Co., Germany) which were calibrated with 5 standard solutions of known pH value in accordance with IUPAC recommendations (Buck et al. 2002). A magnetic stir bar was placed in the beaker of each of the samples in order to homogenize the solution and prevent statistical error. The electrode measured the pH of each sample for at least two minutes before the data was recorded.

3.4.3 Fluoride electrode

A fluoride ion selective electrode was used to measure the concentration of residual fluoride from the columns. A calibration curve was made by recording the potential values for the corresponding fluoride solutions of ten different concentrations: 0.00, 1.25, 2.50, 5.00, 7.50, 10.00, 15.00, 20.00, 25.00, and 30.00 mg/L (table 4, figure 3) Total ionic strength adjustment buffer with a pH of 5.3 was used with fluoride solutions to reduce the interference of other ions (including OH^- and Fe^{3+}). The measured fluoride potentials were used to calculate fluoride concentrations.

Table *4* Standard solutions used for the calibration of the fluoride ion selective electrode

Standard	V_0	V_{TISAB}	$V_{H2O}{}^1$	$V_{H2O}{}^2$	[F]
	(mL)	(mL)	(mL)	(mL)	(mg L^{-1})
1	0.00	20	14	6.00	0.00
2	0.25	20	14	5.75	1.25
3	0.50	20	14	5.50	2.50
4	1.00	20	14	5.00	5.00
5	1.50	20	14	4.50	7.50
6	2.00	20	14	4.00	10.00
7	3.00	20	14	3.00	15.00
8	4.00	20	14	2.00	20.00
9	5.00	20	14	1.00	25.00
10	6.00	20	14	0.00	30.00

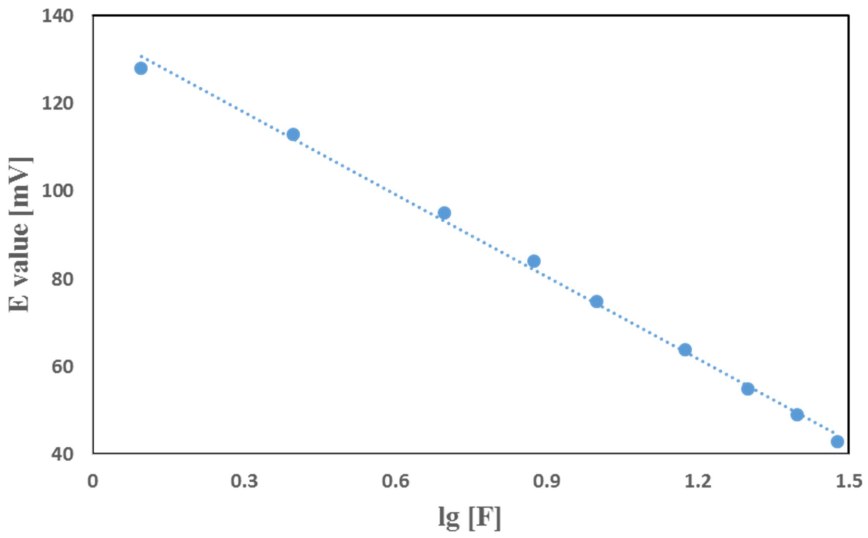

Figure 3. Calibration curve for the electrical potential of the fluoride standard solutions used to determine fluoride concentration in effluent samples.

3.5 Expression of experimental results

3.5.1 Kinetics of Fe^0 oxidative dissolution (k_{EDTA} value)

Given that the initial rate of iron dissolution for each material was expected to follow a linear function ([Fe]t = k_{EDTA}t + b), regression of the experimental data (Fe concentration versus reaction time) allowed calculation of the linear dissolution function for individual materials (Noubactep et al. 2004; Noubactep et al. 2005; Noubactep et al. 2009c; Btatkeu-K et al. 2013b). Direct comparison of the calculated rates of iron dissolution (k_{EDTA}) could be used to indicate the more reactive SW materials, while the calculated intercept ('b') values could be used to indicate the relative amount of pre-existing corrosion products present on the material surfaces. Linear parameters were determined using Origin graphing software.

3.5.2 Discoloration efficiency (E value)

The changes in magnitude of the tested systems for MB and Orange II dyes were calculated and presented as discoloration efficiency percentages (E value). Initial and final concentration of the dyes were determined, and the following formula was used to calculate discoloration efficiency:

$$E = \left[1 - \left(\frac{C}{C_0}\right)\right] * 100\% \qquad \text{(eq. 19)}$$

Where,

C_0= initial concentration of the dye

C= final concentration of the dye

E= discoloration efficiency (%)

4. Results and Discussion

4.1 Iron dissolution in EDTA

4.1.1 Batch experiments

The results of the initial iron dissolution batch experiment performed using 0.1 g SW can be seen in Figure 4. The dissolution rates of each of the SW samples were observed to be similar and therefore not easily distinguishable. The only exception was the stainless steel SW 8, which predictably did not release any dissolved iron due to the non-reactive nature of stainless steel. No expected linear trend was observed in the dissolution rates of the other SW samples, which makes classification of dissolution efficiency difficult. The dissolution rates were calculated for each sample (Table 5; Experiment 1), yet a conclusion based on calculated dissolution rate (k_{EDTA}) would not be practical due to the inconsistent and non-linear nature of the dissolution rate evolution. Therefore the batch iron dissolution experiment was repeated with a modified protocol. The mass used of each steel wool sample was reduced by a factor of 10, with only 0.01 grams being placed in 50 mL of 2 mM EDTA. Figure 4 suggests that the tested materials can be roughly grouped in three different classes: (i) non-reactive (SW8), (ii) low reactive (SW1, SW2, SW3, SW4) and (iii) very reactive (SW5, SW6, SW7).

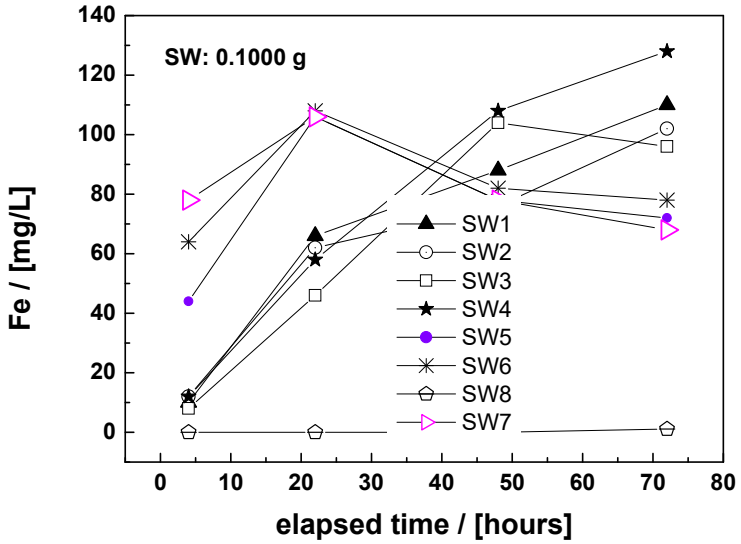

Figure 4. Comparison of the dissolution rate of 0.1 g of the tested SW materials in 2 mM EDTA solution under non disturbed conditions for 72 h. For each material, 0.1 g was used. SW 8 is a stainless steel. The represented lines are not fitting functions, they just connect the points to facilitate visualization. The regression parameters are listed in Table 5.

Table 5 Corresponding correlation parameters (k_{EDTA}, b, R^2) for SW1-SW8. As a rule, the more reactive a material is under given conditions, the higher the k_{EDTA} value. General conditions: 50 mL of 2 mM EDTA solution, at room temperature 22 ± 2 °C, with steel wool mass of 0.1 g (experiment 1) and 0.01 g (experiment 2).

Experiment	Material	R^2	k_{EDTA} ($\mu g h^{-1}$)	b (µg)
Experiment 1	SW 1	0.8984	68.36	186.02
	SW 2	0.9006	60.29	189.91
	SW 3	0.8359	69.15	130.26
	SW 4	0.9578	85.66	139.74
	SW 5	0.0458	9.14	683.29
	SW 6	0.0016	1.24	820.94
	SW 7	0.2712	14.31	929.46
	SW 8	0.6319	0.74	(-) 2.61
Experiment 2	SW 1	0.7975	29.27	264.75
	SW 2	0.8263	28.45	169.31
	SW 3	0.7695	32.67	169.55

	SW 4	0.8159	31.41	182.63
	SW 5	0.8028	28.53	164.41
	SW 6	0.7577	26.79	194.46
	SW 7	0.9770	31.51	95.56
	SW 8	N/A	0.000	0.00

The results of the modified iron dissolution experiment can be seen in Figure 5. Once more it is difficult to distinguish the reactivity rate among the different SW samples, with the exception of the non-reactive SW 8. The calculated dissolution rate (k_{EDTA}) for the 7 reactive samples listed in Table 5 (Experiment 2) show that the SW samples do not vary greatly in the rate of dissolution, with SW 6 having the slowest rate (26.79 $\mu g h^{-1}$) and SW 3 having the fastest rate (32.67 $\mu g h^{-1}$). This means that the reactive steel wool samples have similar rates of corrosion. This could be due to the presence of almost similar amount of corrosion products on the surface of the materials as confirmed by the corresponding b-values. Noubactep et al. (2004; 2005) demonstrated that differences in the reactivity of Fe^0 materials are correlated with differences in the amount of corrosion products on the surface of the materials. The observations in this batch study are consistent with Noubactep's findings. Atmospheric corrosion products on the reactive outer surface of metals suggest that a graphical comparison of materials is not appropriate (Noubactep et al. 2005; Noubactep et al. 2009b; Btatkeu-K et al. 2013a). It appears that the EDTA test is not applicable for powdered (Noubactep et al. 2009b) and therefore very fine SW samples. This seems to suggest that only coarser SW samples (e.g. widths >50 μm) should be used for the EDTA test, and could be considered as the first step in choosing SW for field applications. This observation corroborates the suggestion of Naseri et al. 2017 that only SW materials with a width >50 μm be considered when designing filters.

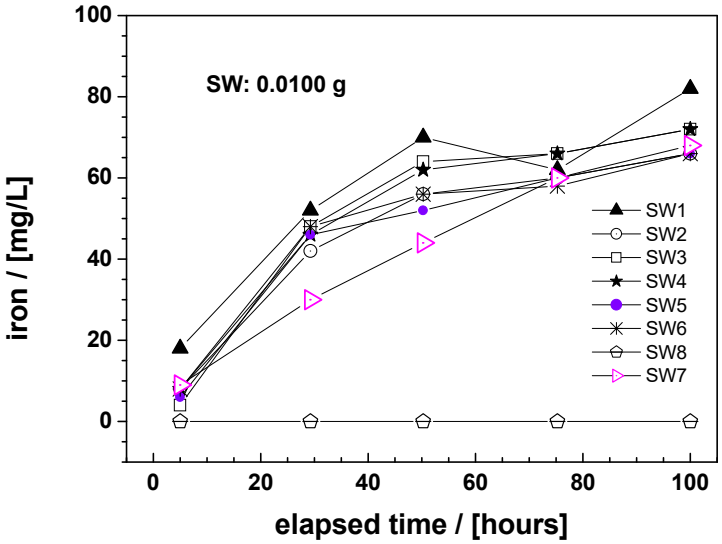

Figure 5. Comparison of the dissolution rate of 0.01 g of the tested SW materials in 2 mM EDTA solution under non disturbed conditions for 72 h. Modified protocol. SW 8 is a stainless steel. The represented lines are not fitting functions, they just connect the points to facilitate visualization. The regression parameters are listed in Table 3.

From figure 4 it can be seen that the "very reactive" specimens show a decrease in iron concentration for experimental durations exceeding 24 hours. The same trend is observed in figure 5 after 40 hours. Because Fe is kept in solution by EDTA, it appears that the maximum stable Fe concentration (saturation) is the one corresponding to 1:1 Fe:EDTA complexation (112 mg L^{-1}). The sooner the maximal Fe concentration is reached the more reactive the material is. This reasoning suggests that SW7 is the least reactive material. However, to achieve better results the experimental duration should be further shortened.

It is therefore reasonable to assume that shortening the duration of the EDTA test for steel wool could be a valuable tool in achieving linearity and better characterizing intrinsic reactivity. Batch experiment 3 was carried out over a thirty hour time period in order to show that a decreased experiment duration could yield better linearity among iron dissolution rates of the SW samples. Two different volumes of EDTA, 50 mL and 100 mL, were used in order to investigate the effect of solution volume on the iron dissolution rate. The graphic results of batch experiment 3 can be seen in figure 6.

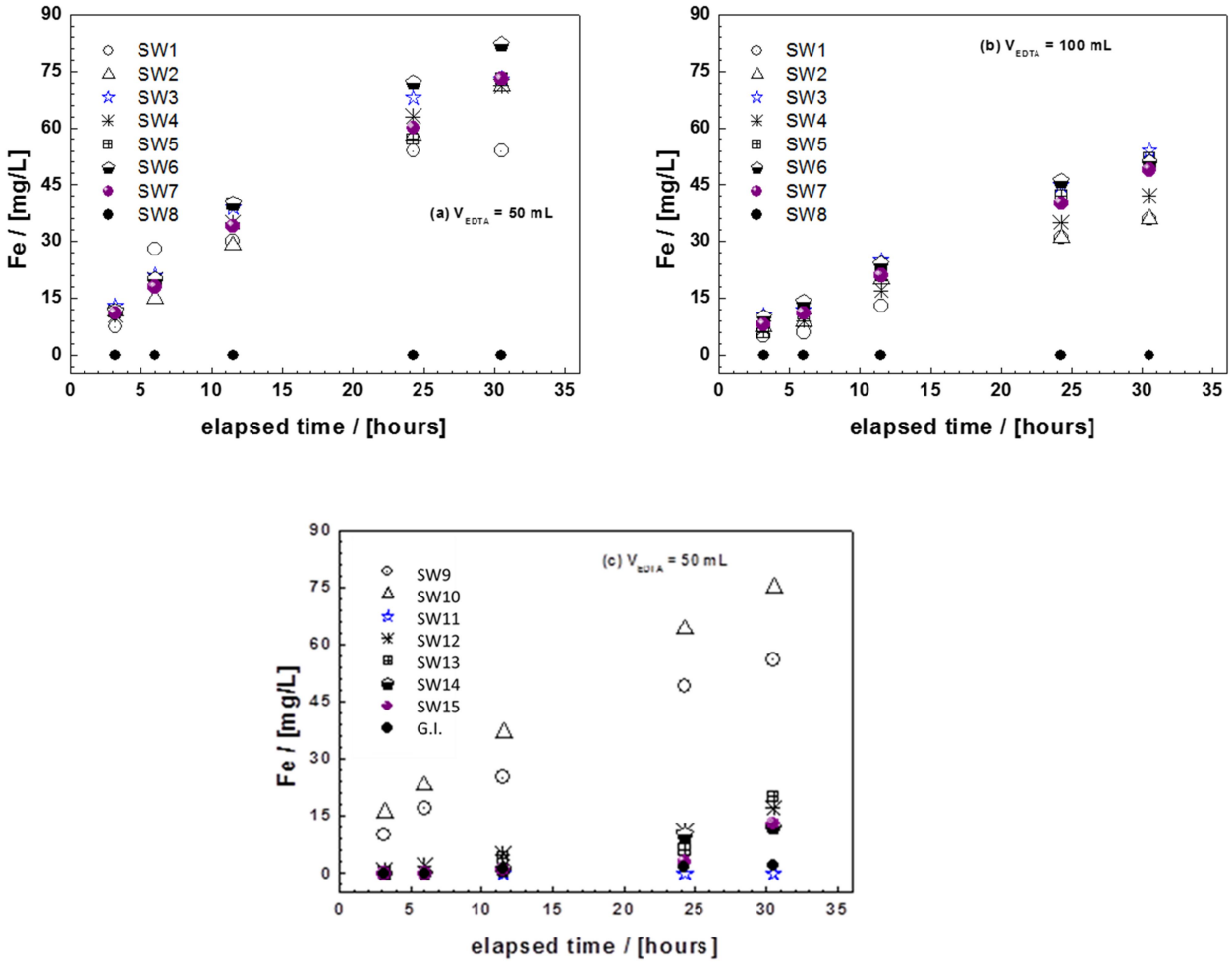

Figure 6. Comparison of the dissolution rate of 0.01 g of the tested SW materials in 2 mM EDTA solution under non disturbed conditions for 30 hours. Three batch tests were performed simultaneously in experiment 3: Using 50 mL of EDTA with SW1-SW8 (a), using 100 mL of EDTA with SW1-SW8 (b), and using 50 mL of EDTA with SW9-SW15 and granular iron (c).

In comparison with batch experiment 1 and 2, better linearity is achieved in all three of the setups of experiment 3. The results of experiment 1 and 2 suggested that improved linearity could be obtained by shortening the duration of the experiment to 25-30 hours, and the results of experiment 3 clearly show that this is indeed the outcome. It is also worth noting that in the case of steel wools 1-8, iron dissolution rate showed somewhat improved linearity, especially for SW1, when the volume of EDTA was increased from 50 mL to 100 mL (figure 6a and 6b). Based on the k_{EDTA} values from experiment 3a (table 6, experiment 3a), the order of highest reactivity for the chosen materials can be considered as: SW6 > SW3 > SW7 > SW2 > SW4 >

SW5 > SW1 > SW8. When the volume of EDTA solution is increased to 100 mL the reactivity order changes slightly, yet a similar reactivity trend is still observed: SW5 > SW3 > SW6 > SW7 > SW4 > SW1 > SW2 > SW8 (table 6, experiment 3b). In both tests, SW6 and SW3 are among the most reactive samples, while SW1, SW4, and SW8 are among the least reactive. These results are similar to the rough classification of reactivity from experiment 1. Experiments 3a and 3b seem to use the best experimental conditions for the EDTA test, therefore the test was extended to the characterization of 7 new SW specimens. Experiment 3c using SW9-SW15 (see table 1) and granular iron yielded results demonstrating good linearity (figure 6c). From the above figure it can be seen that SW10 and SW9 were the most reactive species, yet it is difficult to distinguish among the remaining samples. The resulting k_{EDTA} values help to clarify the reactivity order: SW10 > SW9 > SW13 > SW12 > SW14 > SW15 > GI > SW11 (table 6, experiment 3c).

Table 6. Corresponding correlation parameters (kEDTA, b, R^2) for SW1-SW12 and granular iron. As a rule, the more reactive a material is under given conditions, the higher the kEDTA value. R^2 is a correlation factor. General conditions: 50 mL of 2 mM EDTA solution, 0.01 g Fe^0, SW1-SW8 (experiment 3a), 100 mL of 2 mM EDTA solution, 0.01 g Fe^0, SW1-SW8 (experiment 3b), and 50 mL of 2 mM EDTA solution, 0.01 g Fe^0, SW9-SW15 and granular iron (experiment 3c).

Experiment	Material	R^2	k_{EDTA} ($\mu g h^{-1}$)	b (µg)
Experiment 3a	SW 1	0.8851	78.375	552.90
50 mL EDTA	SW 2	0.9984	111.71	160.04
0.01 g Fe^0	SW 3	0.9761	112.99	435.76
	SW 4	0.9873	110.89	322.41
	SW 5	0.9707	106.88	393.00
	SW 6	0.9881	130.77	282.59
	SW 7	0.996	112.6	261.61
	SW 8	n.a.	0	0
Experiment 3b	SW 1	0.9912	121.37	10.59
100 mL EDTA	SW 2	0.976	106.68	460.98
0.01 g Fe^0	SW 3	0.9937	164.79	444.35
	SW 4	0.9974	132.77	197.41
	SW 5	0.9996	168.14	103.88
	SW 6	0.9908	156.62	537.67
	SW 7	0.9988	152.33	282.43
	SW 8	n.a.	0	0
Experiment 3c	SW9	0.9944	84.91	289.35
50 mL EDTA	SW10	0.997	108.29	516.7

0.01 g Fe^0	SW11	n.a.	0	0
	SW12	0.9838	28.7	77.86
	SW13	0.801	31.22	(-)170.8
	SW14	0.9583	24.43	(-)138.39
	SW15	0.7427	20.07	132.625
	GI	0.9396	3.665	(-)10.31

To consolidate the achieved results, a final iron leaching batch experiment 4 was carried out using one steel wool sample each from Germany, Kenya, and Cameroon, all of the same mass (0.01 g), as well as two samples of granular iron with differing masses (0.1 g and 0.01 g). Testing two different masses of GI aimed at visualizing the importance of adapting the initial conditions to the reactivity of Fe^0 materials. The results of batch experiment 1 and 2 have demonstrated that 0.1 g of SW is too large because saturation is achieved very quickly (see figures 4 and 5 above), the reduction in mass from 0.1 g to 0.01 g did improve the linearity of oxidative iron dissolution rates. Now, 0.01 g of the GI is tested in parallel with 0.1 g to demonstrate the optimal conditions for granular materials does not corresponds to those of fibrous ones. The results of batch experiment 4 can be seen in figure 7. The experiments were performed in triplicates.

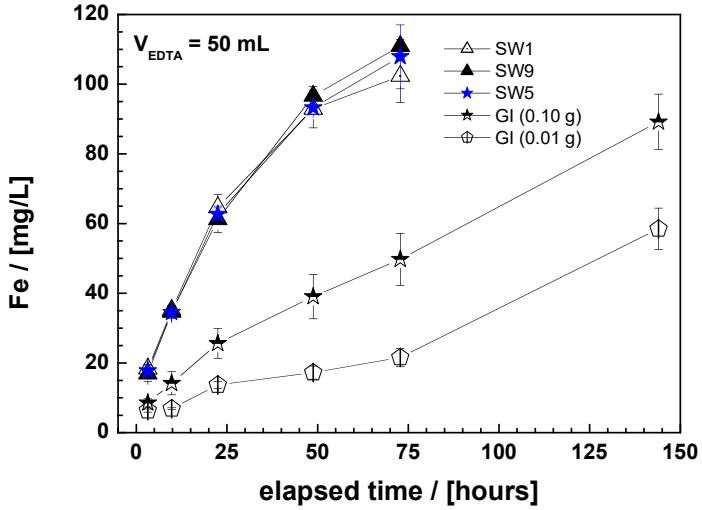

Figure 7. Comparison of three different steel wool specimens and a granular iron sample each weighing 0.01 g, in addition to a granular iron sample weighing 0.1 g. Experimental duration was 150 hours in 50 mL of 2 mM EDTA solution. The investigated SW samples follow a linear trend for iron dissolution rate during the first 25 hours, but not for longer experimental durations. Experimental durations of 96 hours seems to be suitable for the characterization of 0.1 g GI, but not for 0.01 g GI.

During the first 25 hours all of the SW samples show a linear trend in iron dissolution rate. Graphic results show that SW9 is the most reactive specimen, while SW5 is slightly less reactive, and SW1 is the least reactive among the tested SW specimens. All three SW specimens were of the same grade (fine), so the results clearly show that even among Fe^0 materials of the same size/grade there are differences in intrinsic reactivity. For this very reason it is important to screen Fe^0 materials for intrinsic reactivity before use in field applications.

The results show that experimental durations exceeding 30 hours are not suitable for 0.01 g SW, while 96 hours is suitable for 0.1 g GI but not for 0.01 g GI. The longer the experimental duration, the more likely the interference from factors like light (photo-degradation). It appears that increasing the mass of granular iron from 0.01 g to 0.1 g effectively improved the linearity of iron dissolution rate. Because the reactivity rate of granular iron is much lower than the steel wools tested, an increase in mass is a useful tool to increase the concentration of iron in solution. As demonstrated in batch experiment 1 and 2 (figures 4 and 5), a reduction in mass, rather than an increase, is a useful tool for optimizing the linearity of highly reactive samples such as the steel wools tested. In other words, depending on how reactive the sample is, either an increase or decrease in sample mass can be a simple and effective way to improve linearity of iron dissolution rates, and therefore achieve more reliable k_{EDTA} values.

In conclusion, based on the results of the EDTA batch experiments, three effective tools for the optimization of Fe oxidative dissolution rate linearity, and therefore k_{EDTA} values, can be identified: 1.) Decreasing/limiting the duration of the iron dissolution experiment, 2.) Increasing the volume of EDTA, and 3.) Increasing or decreasing the sample mass, depending on sample reactivity. Each of these modifications to the EDTA test have been tested herein and shown to facilitate the characterization of the intrinsic reactivity of steel wool.

4.1.2 Column experiments

Column experiments were carried out based on the results of EDTA batch tests 1 and 2. Neither of the first two batch tests yielded a clear linear trend for the tested materials. Noubactep et al. (2009b) suggested that the materials be compared on the extent of leached Fe in column studies if a distinction cannot be made during batch tests. In column studies, saturation is not expected

and therefore the differential dissolution of Fe^0 materials can be better characterized. As previously mentioned, the results of batch experiment 1 suggest that the materials can be grouped into three different classes: (i) non-reactive (SW8), (ii) low reactive (SW1, SW2, SW3, SW4) and (iii) very reactive (SW5, SW6, SW7). Therefore, one material each from the low reactive and very reactive groups (SW7 and SW1) was then selected. To these two materials from Germany, the two materials (SW5 and SW6) from Kenya were added. SW8 was not considered in these column experiments due to its non-reactive nature. The four selected materials (SW 1, SW 5, SW 6 and SW 7) were of the same grade (Table 1). In addition to the SW specimens, granular iron was also used in the iron leaching column studies as a well-researched reference material. The results of the iron leaching column experiment can be seen below.

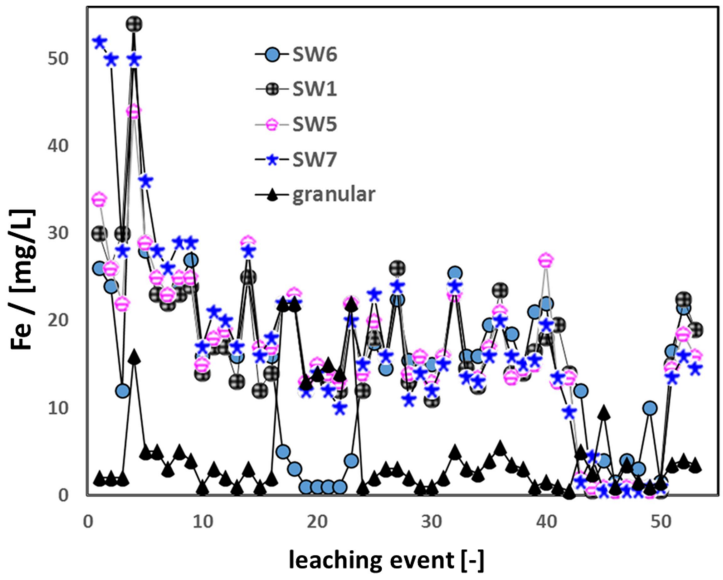

Figure 8. Comparison of leached iron for the five tested Fe^o/sand columns performed for a total of 53 leaching events show that the columns containing SW leached similar concentrations of iron, while GI leached lower concentrations. The iron concentration for each column is recorded as a function of leaching event. The represented lines are not fitting functions, they just connect the points to facilitate visualization

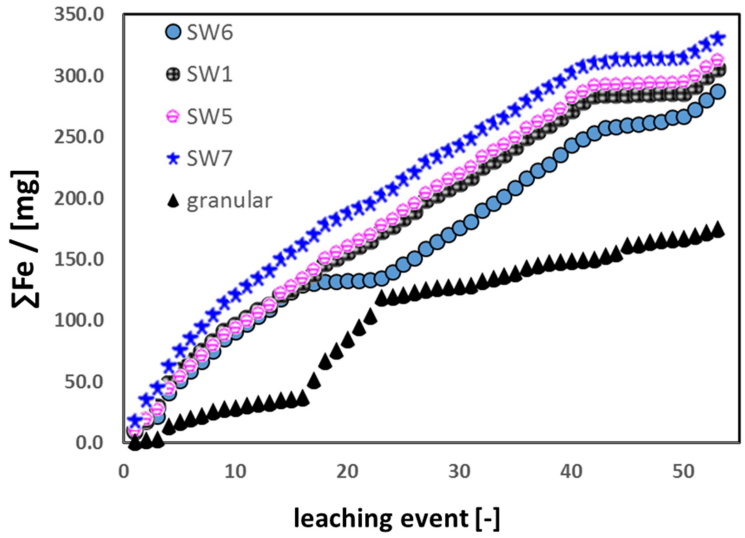

Figure 9. Comparison of the cumulative mass of leached iron from each column shows that SW7 released the greatest mass of iron over the experimental duration, while GI leached the smallest mass. Cumulative mass of iron is recorded as a function of leaching event. Looking at the cumulative mass totals helps to distinguish the columns from one another in regards to reactivity.

Figure 8 shows the results of iron concentrations recorded as a function of leaching event from the selected materials during the iron leaching column studies. Although all of the SW systems leached similar amounts of iron concentration per leaching event, a closer inspection of the graphic results suggests that the SW 7 column had higher concentrations of leached Fe than the other SW systems. This observation can be clearly seen in figure 9, which shows that the cumulative mass of Fe release was greater for the SW7 system than the other SW systems and granular iron. SW6 displays a net decrease of the kinetic of dissolution after 16 leaching events, as well as after 44 leaching events. This documents the lack of linearity in the kinetics of Fe^0 oxidative dissolution even under conditions where no oxides/hydroxides precipitate. All of the investigated SW specimens show a net decrease of the kinetic of dissolution after 44 leaching events, and an increase after 49 leaching events, also documenting the lack of linearity of the kinetics of Fe^0 oxidative dissolution. Careful inspection of figure 8 also shows that in addition to the initial high concentration of leached Fe, a large spike in Fe concentration occurs after 4 leaching events for all columns. This is due to a longer residence time of the EDTA solution in the columns before the columns could be drained and effluent samples taken. Columns were usually drained and the effluent analyzed every 1-4 days (figure 10), however a period of 24 days passed between the 4^{th} and 5^{th} leaching events, leading to an increase in Fe concentration

above the initial concentrations due to the increased contact time of EDTA and Fe^0 samples. This accounts for the high Fe concentration anomaly.

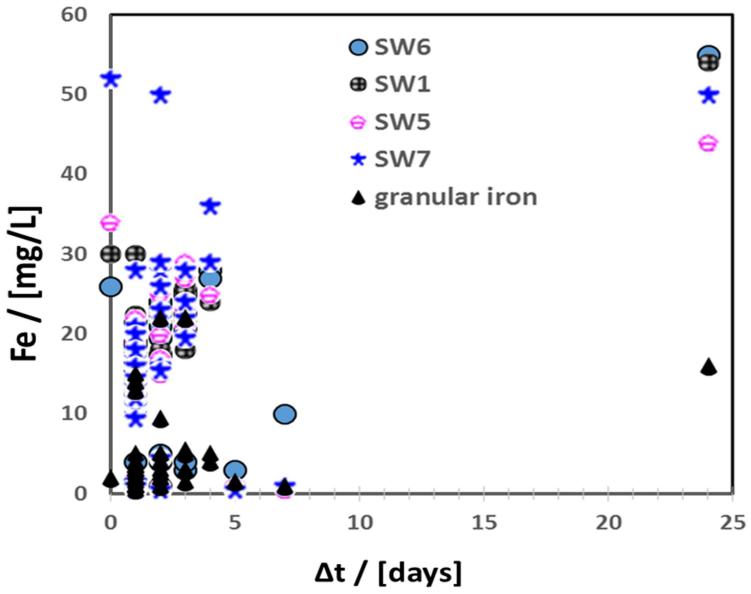

Figure 10. Leaching events usually occurred every 1-4 days, but 24 days passed between the 4th and 5th leaching event, leading to a spike in Fe concentrations greater than initial conditions.

Table 7 shows the initial Fe concentrations and cumulative mass of leached iron for each of the SW systems and granular iron at 16 and 53 leaching events, and confirms quantitatively that the SW 7 column leached the greatest mass of iron (330.9 mg) by the end of the experiment. Among the four SW specimens, the cumulative mass of leached Fe was smallest for SW 6 (287.3 mg). SW 5 and SW 1 leached a cumulative mass of Fe of 313.9 mg and 306.3 mg, respectively. Granular iron leached a much smaller mass of iron than the tested SW specimens (175 mg). This result is supported by the low k_{EDTA} value of granular iron in comparison to the SW specimens in the iron dissolution batch experiments (see table 6 above). Even after only 16 leaching events, the order of reactivity was the same as after 53 leaching events, regardless of what parameter is considered: SW7 > SW5 > SW1 > SW6 > GI. The results show that even though the tested SW systems can be differentiated based on their reactivity better than in the iron dissolution batch

tests in EDTA, it would still be difficult to confidently select one SW system for further investigation and field experiments due to the similarity among the experimental data for all four tested SW systems. In other words, long-term experiments might still be necessary to establish a stable and conclusive reactivity order despite the clear differentiation (figure 9). The absence of a linear trend describing the materials dissolution rate and its repeatability throughout the duration of this iron leaching column experiment signifies that SW is not a homogeneous class of Fe^0 material.

Table 7. Initial iron concentration ($[Fe]_0$) and extent of iron leaching after 16 and 53 leaching events. $\sum m$ is the cumulative mass of leached iron, and P is leached iron as a percentage of initial mass. The initial mass of each steel wool was 500 mg. It is seen that the order of reactivity is the same regardless of which parameter is considered.

Parameter	**Unit**	**SW6**	**SW1**	**SW5**	**SW7**	**G.I.**
$\mathbf{[Fe]_0}$	(mg/L)	26.0	30.0	34.0	52.0	2.0
$\mathbf{\Sigma m_{16}}$	(mg)	128.9	130.9	135.3	162.5	37.2
$\mathbf{P_{16}}$	(%)	25.8	26.2	27.1	32.5	7.4
$\mathbf{\Sigma m_{53}}$	(mg)	287.3	306.3	313.9	330.9	175.0
$\mathbf{P_{53}}$	(%)	57.5	61.3	62.8	66.2	35.0

It is important to emphasize that due to the nature of complex interactions within the "Fe^0-contaminant- water" system, even when a clear and distinguishable reaction order can be observed among the tested materials, the most reactive material is not necessarily the most suitable for field applications. In fact, a highly reactive material would likely produce more corrosion products and other precipitates which could decrease filter lifespan and lead to its passivation. It could actually be advantageous to select a less reactive material, such as SW 6, which would enable a longer filter lifespan and long term satisfactory use. The ideal approach of selecting materials of similar reactivity for filter use, in addition to iron dissolution studies, would be to test the materials for individual contaminants specific to the water quality goals. For practical purposes, it should also be noted that when the reactivity of the tested materials is similar among all SW systems, then the material with the cheapest cost would be the most advantageous selection for decentralized water treatment.

4.2 Dye discoloration experiments

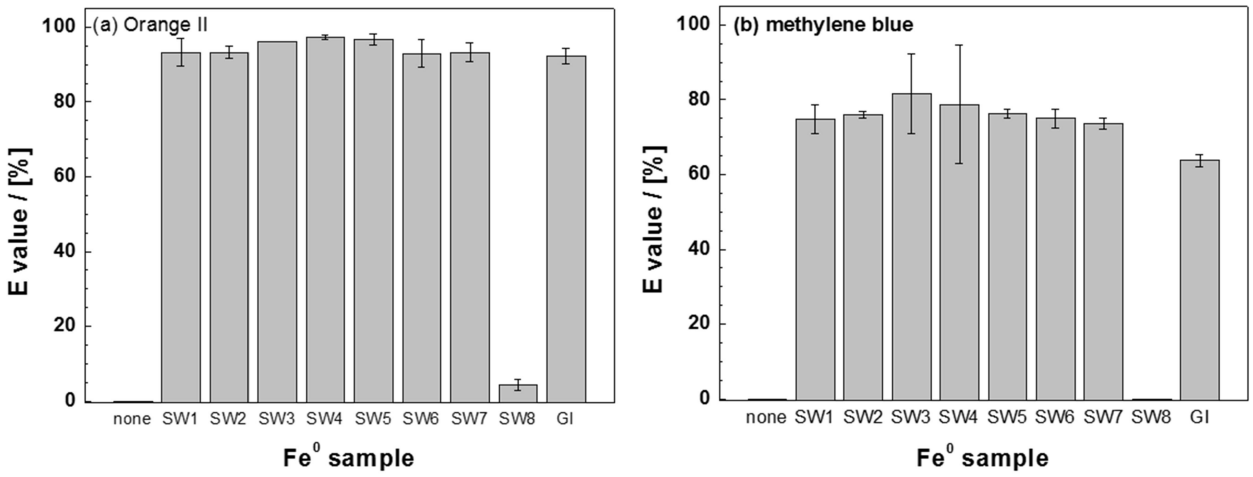

Figure 11. Comparison of discoloration efficiency for SW1-SW8 and GI in Orange II (a) and Methylene Blue (b). Experimental conditions: 0.05 g Fe^0; 22 mL of dye at concentration of 10 mg/L; rotational shaking for 8 weeks at 75 rotations per minute. Orange II was discolored more efficiently than MB by all reactive samples.

Figure 11 shows the results of the 8 week dye discoloration batch experiments with Orange II and MB. Except for the stainless steel sample SW8, all other samples had a discoloration efficiency greater than 90% for Orange II (Table 8). For MB however, discoloration efficiency for all samples was much less in comparison to Orange II, with SW3 showing the greatest MB discoloration (81.67%). These results support the idea that Fe^0 produces *in-situ* positive charged oxides and hydroxides. The anionic Orange II is attracted to and adsorbed onto the positively charged corrosion products, leading to its discoloration. Positively charged MB was also discolored. This can be attributed to the weak adsorption of MB onto positively charged iron oxides and the following co-precipitation (Phukam 2015).

Table 8. Comparison of discoloration efficiencies of SW1-SW8 and GI for Orange II and Methylene Blue after 8 weeks of rotational shaking at 75 rpm.

Sample	Orange II	MB
(-)	E (%)	E (%)
Ref.	0.0	0.0

SW1	93.3	74.7
SW2	93.3	76.0
SW3	96.0	81.7
SW4	97.3	78.7
SW5	96.7	76.3
SW6	93.0	75.0
SW7	93.3	73.7
SW8	4.3	0.0
GI	92.3	63.7

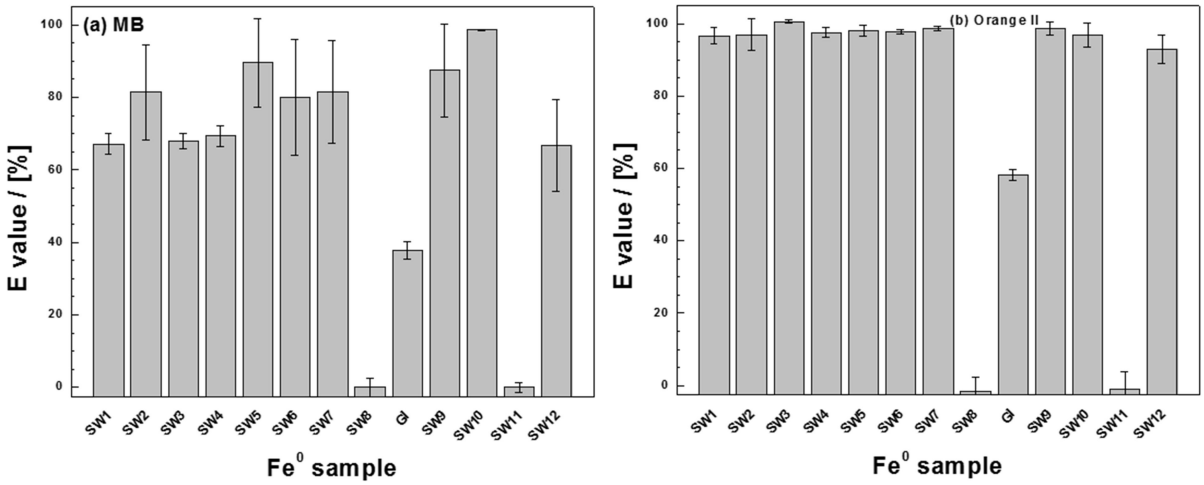

Figure 12. Comparison of discoloration efficiency for SW1-SW12 and GI in Methylene Blue (a) and Orange II (b). Experimental conditions: 0.05 g Fe^0; 22 mL of dye at concentration of 10 mg/L; rotational shaking for 2 weeks at 75 rotations per minute.

Figure 12 shows the results of the second dye discoloration batch experiment lasting for 2 weeks, which was extended to four additional SW specimens (SW9, SW10, SW11, and SW12). As with the first dye discoloration batch experiment, a better discoloration efficiency was observed for Orange II than MB for almost all steel wool samples, with the exception of SW10, which actually showed a better discoloration efficiency for MB rather than Orange II (96.9% for Orange II; 98.6% for MB). This shorter duration experiment supports the results of the 8 week batch experiment, showing that the anionic Orange II is more strongly adsorbed onto positively charged iron oxide corrosion products than cationic MB. With the exception of stainless steel samples SW8 and SW11, and granular iron, the other steel wool samples each displayed a discoloration efficiency of more than 90% for Orange II. Discoloration efficiency was less for

MB, and yet even so, every reactive steel wool sample showed a discoloration efficiency greater than 65%. Of all reactive samples, GI had the lowest discoloration efficiency for both Orange II and MB, at 58.2% and 37.7%, respectively (Table 9). The lower discoloration efficiency of GI, in comparison to SW, reflects the low reactivity (k_{EDTA}) of GI as demonstrated in the batch and column iron leaching experiments (Tables 6 and 7).

Table 9. Discoloration efficiencies of SW1-SW12 and granular iron for Orange II and Methylene Blue after 2 weeks of rotational shaking at 75 rpm. The values presented below are the averages of each triplicate set of Fe^0 material.

Sample	Orange II	MB
(-)	E (%)	E (%)
Ref.	0.0	0.0
SW1	96.7	67.2
SW2	97.0	81.4
SW3	100.0	68.0
SW4	97.6	69.4
SW5	98.0	89.6
SW6	97.8	80.1
SW7	98.6	81.4
SW8	0.0	0.0
GI	58.2	37.7
SW9	98.7	87.5
SW10	96.9	98.6
SW11	0.0	0.0
SW12	92.9	66.7

In summary, steel wool and GI are more effective at discoloring anionic Orange II due to the attractive nature of positively charged iron-oxide corrosion products and negatively charged Orange II ions. Due to the weak adsorption of MB onto the iron-oxides, MB discoloration is also observed in the presence of Fe^0-bearing materials. Based on these results, it appears that steel wool is a viable option for the removal of negatively charged contaminants, as well as positively charged contaminants to a lesser degree, in use with water filters. Therefore fluoride was chosen as an anionic contaminant to be tested for removal efficiency in use with SW/sand filters in column studies.

4.3 Application: Fluoride removal

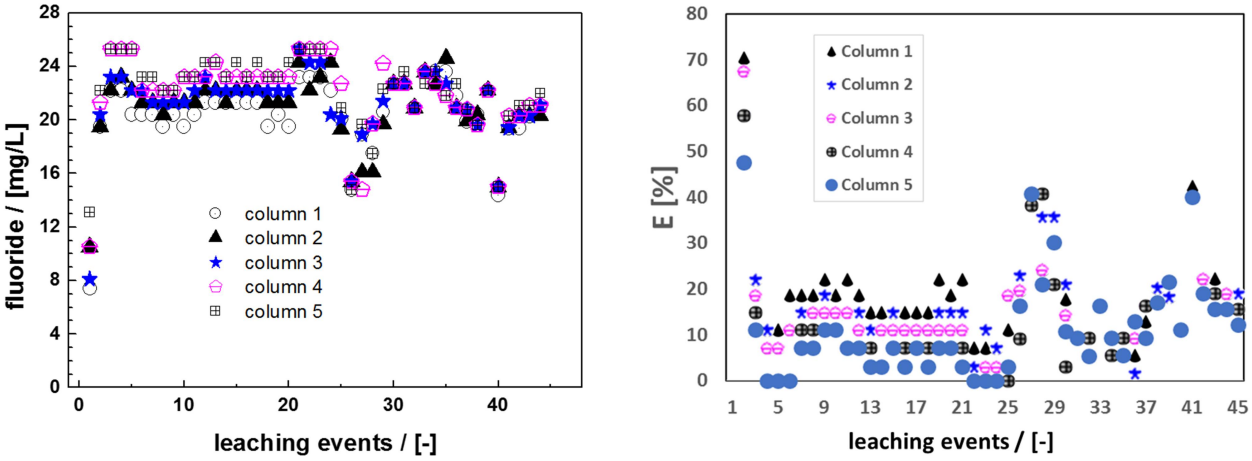

Figure 13. Comparison of the five tested columns for fluoride removal. The results of the fluoride column experiment are recorded for each column as fluoride concentration as a function of leaching event (a), and fluoride removal efficiency as a function of leaching event (b).

Table 10. Comparison of average fluoride removal efficiency for the five tested columns shows that Column 1 had the greatest removal efficiency, while Column 5 had the least. Average fluoride removal efficiency is shown as the average percentage of each column after 44 leaching events.

Average Fluoride removal	**(%)**
Column 1	18.3
Column 2	16.6
Column 3	15.2
Column 4	12.3
Column 5	11.2

Figure 13 summarizes the concentration of F^- measured in the columns during 44 leaching events, as well as the average removal efficiency of F^- by each SW/sand system. From figure 13b it appears that column 4 and column 5 were the least efficient at removing F^-. This observation is supported by the calculated average F^- removal efficiency for each column (table 10). Column 5 had an average removal efficiency of only 11.2%, while column 4 had only a slightly better removal efficiency of 12.3%. Column 1 had the highest average F^- removal efficiency (18.3%), while Column 2 and Column 3 had a removal efficiency of 16.6% and 15.2%, respectively. Therefore an F^- removal efficiency order can be established: column 1 > column 2 > column 3 >

column 4 > column 5. The mass of steel wool in each column was 2 g, so the resulting differences in effectiveness at F^- removal must be attributed to the intrinsic reactivity of each steel wool sample. The results also indicate that steel wool is a potentially effective material for mitigating F^-. For these experiments, it is assumed that the sand in the filters acts only as a control system and does not play a large role in F^- removal, since the mass of sand used in each column was equal. This assumption is made for the simplification of result interpretation. The reasoning behind this assumption is that the chemical potential gives preferentiality to Fe^{2+} adsorption at the surface of sand, leading to *in-situ* coating. The surface is destroyed by chemical reactions leading to *in-situ* coating, which allows for competitive adsorption at the surface of newly formed molecules, like Fe $(OH)_2$, for example. Fe^0 should theoretically not be able to reduce F^-, as the corresponding electrode potential values for Fe^0 and F^- are $E^0 = -0.44$ V and $E^0 = 2.87$ V, respectively. Therefore the resulting removal of F^- from the columns can be attributed to adsorption (Ndé-Tchoupé et al. 2015).

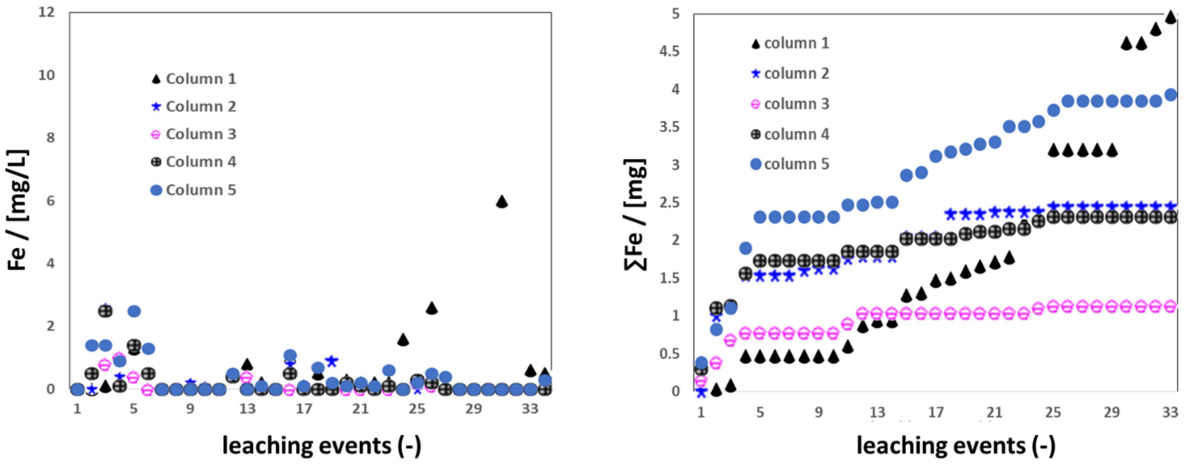

Figure 14. The concentration of leached iron for all columns was low after the first 6 leaching events (a), making direct comparisons among columns difficult. The mass of leached iron as a function of leaching event (b) allows distinctions to be made among the columns.

Figure 14 summarizes the evolution of iron dissolution in the effluent from the columns. Measured iron concentrations were low throughout most of the experimental duration, making comparisons among columns difficult. However, a look at the cumulative mass of leached Fe

provides more insight into the functionality of each column. At the end of the experiment, column 3 had released the lowest mass of Fe (1.13 mg), while column 1 released the greatest mass (4.96 mg). Column 2, column 4, and column 5 released 2.44 mg, 2.31 mg, and 3.94 mg Fe, respectively. After the first 6 leaching events, the iron concentration in the effluent is nearly negligible, and this is reflected in the cumulative leached Fe totals (table 11), which shows that after reaching a certain cumulative mass, most of the columns no longer leach an appreciable amount of Fe. The exception is column 1, which displays an increase in total leached Fe during the last few leaching events. This could be explained by the longer residence time of the water in the columns. Instead of samples being taken every 1-2 days, samples were not able to be taken as frequently during the final leaching events, with 3-6 days passing between samplings. This allowed for a relatively higher accumulation of Fe in the columns before the effluent could be collected. Although iron dissolution during this time of less frequent sampling is not reflected in the cumulative Fe mass of the other columns, an increased reduction in F^- for all systems did occur. Increased residence time seems to explain the spike in F^- removal efficiency around the 28^{th} and 40^{th} leaching events (figure 13b).

Table 11. Cumulative mass of Fe reflects the total mass of leached Fe from each column.

Total Cumulative Mass Fe^0	**(mg)**
Column 1	4.96
Column 2	2.44
Column 3	1.13
Column 4	2.31
Column 5	3.94

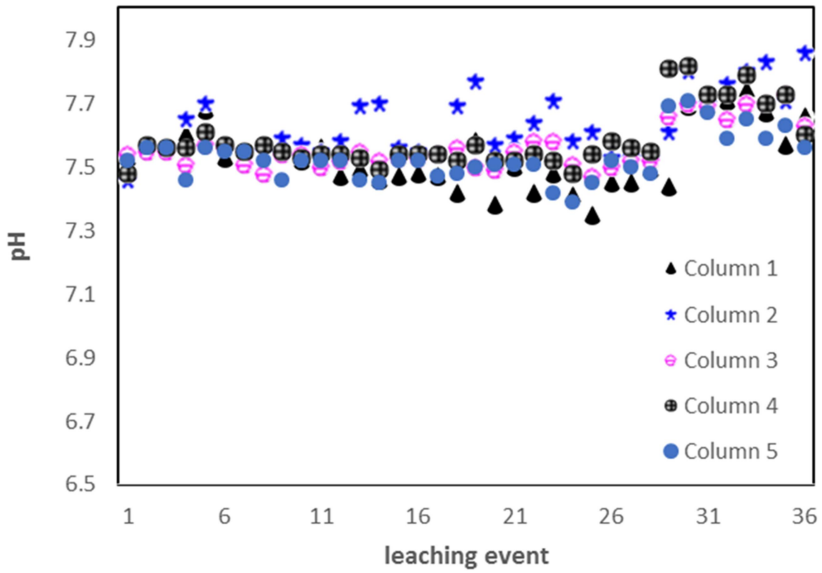

Figure 15. pH was recorded as a function of leaching event for each of the investigated column systems. Experimental conditions: 2g steel wool per column; initial fluoride concentration is 25 mg/L.

Figure 15 shows the evolution of pH for each column. In general, it can be seen that column 2 had a higher average pH than the other column systems, with some values exceeding 7.7. Apart from a few pH fluctuations, most of the columns exhibited pH values between 7.4 and 7.6 for the first 28 leaching events. After 28 leaching events, an increase in pH is observed for all column systems. This is most likely due to a decreased sampling frequency. At the beginning of the experiment, sampling was performed every 1- 2 days. However, there was a 6 day delay between the 28th and 29th leaching event, and a 4 day delay between the 29th and 30th leaching event. The increase in pH is therefore most likely explained by the longer residence times of water in the column and longer contact time of the water with steel wool, leading to a buildup of HO^-. Throughout the experimental duration, all columns exhibited pH > 7.0. Adsorption at this pH range is preferential at the surface of positively charged iron oxides rather than at the negatively charged surface of sand grains (Btatkeu-K et al. 2014).

At the end of the experiment, all columns exhibited reddish-brown discoloration within and surrounding the reactive zone (figure 16), demonstrating that iron hyrd(oxides) had been produced and subsequently precipitated from solution. No calculations of porosity or hydraulic conductivity were carried out for these experiments, as the goal of this experiment was not to characterize porosity loss over time.

Figure 16. Brown discoloration within and surrounding the reactive zone indicate that iron corrosion products formed and were precipitated. The blue solution within the column is Methylene Blue, which was added at the end of the experiment as part of a subsequent experiment not included in the present work.

It is worth noting that column 1 (containing SW1) had the highest fluoride removal efficiency among the tested specimens, but had a low k_{EDTA} value in the batch experiments because of its lower reactivity in comparison to the other steel wool specimens (see table 6 above). In this case, column 1 had the highest fluoride removal efficiency because it was not as reactive as the other specimens and therefore not passivated as quickly, leading to a longer and more effective lifetime of the contaminant removal system. Column 5 (containing SW6), on the other hand, had a very high k_{EDTA} value because of its reactive nature, but showed the lowest fluoride removal efficiency. This result demonstrates the fact that when choosing Fe^0 materials for field applications, the most reactive specimen is not necessarily the best selection for contaminant removal. It is for this reason that screening of Fe^0 materials is of critical importance.

Despite a significant amount of fluoride removal by SW in column studies, effluent fluoride concentrations were still above the 1.5 g/L limit set by the WHO for safe drinking water. Further

research should be directed at optimizing fluoride removal by SW, as well as the removal of other contaminant species. The effect of additional ions on fluoride removal in Fe^0 filters is currently being investigated (Heimann 2018; Heimann et al. 2018)

5. Conclusions

The present work has shown that the selection of SW, or any Fe^0 material, is not always a straight-forward and obvious decision. The parameter k_{EDTA} was used as a simple and effective way to facilitate the characterization of a material's intrinsic reactivity and be able to compare the reactivity of Fe^0 samples from different sources. The present study has made modifications to the protocol for intrinsic reactivity characterization of Fe^0 materials in order to make it suitable for a more reactive Fe^0 material like SW. The modifications include:

(i) Decreasing/limiting the experimental duration
(ii) Increasing the volume of EDTA
(iii) Decreasing the mass of SW

These modifications were shown to be effective at establishing a more linear rate of iron dissolution and therefore more reliable k_{EDTA} value. Because SW is more reactive than many other Fe^0 materials like granular iron, the rate of iron dissolution for SW is not linear and does yield a reliable k_{EDTA} value when used with the protocol of Noubactep et al. (2004) for the characterization of intrinsic reactivity in 2 mM EDTA solution.

K_{EDTA} values obtained using the modified protocol allowed for characterization of SW specimens and facilitated the selection process of SW specimens to be used in subsequent iron leaching column experiments. The column experiments were performed in order to better distinguish the reactivity of SW specimens that displayed similar iron dissolution rates in batch experiments. This is a valuable tool for the selection of Fe^0 materials that are to be used for long-term filter use.

When considering the contaminant removal efficiency of individual contaminants by SW, the proposed approach can be applied for the screening of SW for the quick selection of materials that are most effective for specific conditions. Because the reactivity of SW depends on many factors such as chemical composition, surface area, surface roughness, corrosion state, as well as manufacturing characteristics like heat treatment, the only means of determining these effects on contaminant removal is to investigate SW under the appropriate settings.

The present study can be considered as an initial effort to characterize the intrinsic reactivity of SW, which could be used to improve screening protocols for Fe^0 materials for application in water filters. Moreover, this study suggests that a standard protocol for the screening of SW materials is needed. The results of this work suggest that k_{EDTA} values should be used to support the reasonable selection of Fe^0 materials and to ease comparison of results from different sources. Further research could be directed at investigating the effects of coating on SW materials and how iron dissolution is affected with and without pre-treatment in acid, thereby improving the protocol for SW intrinsic reactivity characterization.

References

Abramiam, L.; El-Rassy, H. (2009): Asorption kinetics and thermodynamics of azo-dye Orange II onto highly porous titania aerogel. In: Chemical Engineering Journal 150 ((2-3)), Pg. 403–410.

Alyoussef G. (2018): Characterizing the Impact of Contact Time in Investigating Processes in Fe0/H2O systems. Freiberg Online Geoscience (In press).

Arai, Takeo; Yanagida, Masatoshi; Konishi, Yoshinari; Sugihara, Hideki; Sayama, Kazuhiro (2008): Utilization of Fe3+/Fe2+ Redox for the Photodegradation of Organic Substances over WO3 Photocatalyst and for H2 Production from the Electrolysis of Water. In: Electrochemistry (2),p 128–131.

Asgari, G.; Ramavandi, B.; Farjadfard, S. (2013): Abatement of Azo Dye from Wastewater Using Bimetal Chitosan. In: The Scientific World Journal.

Banerji, T.; Chaudhari, S. (2017): A cost-effective technology for arsenic removal: case study of zero valent iron-based IIT Bombay arsenic filter in West Bengal. In Nath K, Sharma V. (eds) Water and Sanitation in the New Millenium. New Delhi, DOI: https://doi.org/10.1007/978-81-322 3745 7_11.: Springer.

Bharati, P.; Kupakaddi, A.; Rao, M.; Naik, R. (2005): Clinical Symptoms of Dental and Skeletal Fluorosis in Gadag and Bagalkot Districts of Karnataka. In: Journal of Human Ecology 18 (2), pg. 105- 107.

Birke, V.; Schuett, C.; Burmeier, H.; Friedrich, H-J (2015): Impact of trace elements and impurities in technical zero-valent iron brands on reductive dechlorination of chlorinated ethenes in groundwater. Boca Raton, Florida, USA: CRC Press.

Bojic, A.; Purenovic, M.; Bojic, D. (2004): Removal of chromium (VI) from water by micro-alloyed aluminum composite (MAIC) under flow conditions. In: Water SA 30 (3), pg. 353–359.

Bojic, A.; Purenovic, M.; Kocic, B.; Perovic, J.; Ursic-Jankovic, Bojic, D. (2001): The inactivation of Escherichia Coli by microallayed aluminum based composite. In: Facta Universitatus: Physics, Chemistry, and Technology 2 (3), pg. 115–124.

Btatkeu-K, B. D.; Miyajima, K.; Noubactep, C.; Care, S. (2013a): Testing the suitability of metallic iron for environmental remediation: Discoloration of methylene blue in column studies. In: Chemical Engineering Journal 215-216, pg. 959–968.

Btatkeu-K, B. D.; Miyajima, K.; Noubactep, C.; Care, S. (2013b): Testing the suitability of metallic iron for environmental remediation: Discoloration of methylene blue in column studies. In: Chemical Engineering Journal 215-216, pg. 959–968.

Btatkeu-K, B. D.; Olvera-Vargas, H.; Tchatchueng, J. B.; Noubactep, C.; Care, S. (2014): Determining the optimimun Fe0 ratio for sustainable granular Fe0/sand water filters. In: Chemical Engineering Journal (247), pg. 265–274.

Buck, R. P.; Rondinini, S.; Covington, A. K.; Baucke, F.G.K.; Brett, C.M.A., Camoes, M.F.; Milton, M.J.T. et al. (2002): Measurement of pH. Definition, Standards, and Procedures. IUPAC Recommendations 2002. In: Pure Appl. Chem. 74 (11), pg. 2169–2200.

Caré, S.; Crane, R.; Calabro, P.; Noubactep, C. (2013): Modelling the Permeability Loss of Metallic Iron Water Filtration Systems. In: CLEAN- Soil, Water, Air 41 (3), S. 275–282.

Caré, S.; Nguyen, Q. T.; L'hostis, V.; Berthaud, Y. (2008): Mechanical properties of the rust layer induced by impressed current method in reinforced mortar. In: Cement and Concrete Research 38 (8-9), pg. 1079–1091.

Comba, S.; Di Molfetta, A.; Sethi, R. (2011): A comparison between field applications of nano-, micro-, and millimetric zero valent iron for the remediation of contaminated aquifers. In: Water, Air, and Soil Pollution 215, pg. 595–607.

Crawford, R. J.; Harding, I. H.; Mainwaring, D. E. (1993): Adsorption and Coprecipitation of Single Heavy Metal Ions onto the Hydrated Oxides of Iron and Chromium. In: Langmuir 9, pg. 3050 -3056.

Diao, M.; Yao, M. (2009): Use of zero-valent iron nanoparticles in inactivating microbes. In: Water Resources 43 (20), pg. 5243–5251.

Dickerson, R. E.; Gray, H. B.; Haight, G. P. (1979): Chemical Principles (3rd Edition). Menlo Park, CA: Benjamin/Cummings Publishing Company Inc.

DOE (1993): DOE Fundamentals Handbook: Volume 1 of 2.

Domga, R.; Tongue-Kamga, F.; Noubactep, C.; Tchatchueng, J. B. (2015): Discussing porosity loss of Fe0 packed water filters at ground level. In: Chemical Engineering Journal 263, pg. 127–134.

Ebelle T.C., Makota S., Tepong-Tsindé R., Nassi A., Noubactep C. (2018): Metallic iron and the dialogue of the deaf. Fresenius Environmental Bulletin (In press).

Erickson, A. J.; Weiss, P. T.; Gulliver, J. S. (2007): Enhanced Sand Filtration for Storm Water Phosphorus Removal. In: Journal of Environmental Engineering, ASCE 133, pg. 485–497.

Evans, R. U. (1939): Korrosion, Passivität und Oberflächenschutz von Metallen. Berlin, 742 pp: Springer.

Fawell, J.; Bailey, K.; Chilton, J.; Dahi, E.; Fewtrell, L.; Magara, Y. (2006): Fluoride in Drinking Water. In: World Health Organization (WHO), pg. 1–134.

Gaun, X.; Sun, Y.; Qin, H.; Li, J.; Lo, I. M. C.; He, D.; Dong, H. (2015): The limitations of applying zero valent iron technology in contaminants sequestration and the corresponding countermeasures: The development in zero-valent iron technology in the last two decades (1994 -2014). In: Water Research 75, pg. 224–248.

Ghauch, A.; Abou Assi, H.; Baydoun, H.; Tuqan, A.; Bejjani, A. (2011): Fe0 -based trimetallic systems for the removal of aqueous diclofenac: Mechanisms and kinetics. In: Chemical Engineering Journal 172 (2-3), pg. 1033–1044.

Ghauch, A.; Abou Assi, H.; Tuqan, A. (2010): Investigating the mechanism of clofibric acid removal in Fe0/H2O systems. In: Journal of Hazardous Materials 176 (1-3), pg. 48–55.

Gheju, M. (2018): Progress in understanding the mechanism of CrVI Removal in Fe0-based filtration systems. In: Water 10 (651). Online verfügbar unter doi:10.3390/w10050651.

Gheju, M.; Balcu, I. (2011): Removal of chromium from Cr(VI) polluted wastewaters by reduction with scrap iron and subsequent precipitation of resulted cations. In: Journal of Hazardous Materials 196 (131-138).

Gheju, M.; Balcu, I. (2019): Sustaining the efficiency of the Fe(0)/H2O system for Cr(VI) removal by MnO2 amendment. Chemosphere 214, pg. 389-398.

Ghosemi, J.; Asadpour, S. (2007): Thermodynamics studies of the adsorption process of methylene blue on activated carbon at different ionic strengths. In: Journal of Chemical Thermodynamics 39, pg. 967–971.

Gillham, R. W.; O'Hannesin, S. F. (1994): Enhanced Degradation of Halogenated Aliphatics by Zero Valent Iron. In: Ground Water 32 (6), pg. 958–967.

Gillham, R. W.; O'Hannesin, S. F. (1998): Long-Term Performance of an In-Situ "Iron Wall" for Remediation VOC's. In: Ground Water 36 (1), pg. 164–170.

Gottinger, A, M.; McMartin, D. W.; Wild, D. J.; Moldovan, B. (2013): Integration of zero valent iron sand beds into biological treatment systems for uranium removal from drinking water wells in rural Canada. In: Canadian Journal of Civil Engineering 40 (10), pg. 945–950.

Gunawardana, B.; Singhal, N.; Swedlund, P. (2011): Degradation of Chlorinated Phenols by Zero Valent Iron and Bimetals of Iron: A Review. In: Environmental Engineering Research 16 (4), pg. 187 203.

Heimann, Svenja (2018): Testing Granular Iron for Fluoride for Aqueous Fluoride Removal. Freiberg Online Geoscience 52, 80 pp.

Heimann S., Ndé-Tchoupé A.I., Hu R., Licha T., Noubactep C. (2018): Investigating the suitability of Fe0 packed-beds for water defluoridation. Chemosphere 209, 578–587.

Henderson, A. D.; Demond, A. H. (2007): Long-Term Performance of Zero-Valent Iron Permeable Reactive Barriers: A Critical Review. In: Environmental Engineering Science 24 (4), pg. 401 423.

Hilberg, S. (2015): Umweltgeologie: Eine Einfuhrung in Grundlagen und Praxis. Heidelberg: Springer Spektrum.

Hildebrant, B.; Ndé-Tchoupé, A. I. (2018): Potentials of available Fe0 materials as filters media: The suitability of steel wool. In: In publication.

Holdrich, R. G. (2002): Fundamentals of particle technology: Shepshed: Midland Information Technology and Publishing, 173 pp.

Hussam, A. (2009): Contending with a developing disaster: SONO filters remove arsenic from well water in Bangladesh. In: Innovations 4, pg. 89–102.

Hussam, A.; Munir, A. K. (2007): A simple and effective arsenic filter based on composite iron matrix: development and deployment studies for groundwater of Bangledesh. In: Journal of Environmental Science and Health Part A 42 (12), pg. 1869–1878.

Imamura, K.; Ikeda, E.; Nagayasu, T.; Sakiyama, T.; Nakanishi, K. (2002): Adsorption Behavior of Methylene Blue and its Congeners on a Stainless Steel Surface. In: Journal of Colloid and Interface Science 245, pg. 50–57.

James, B.; Rabenhorst, M.; Frigon, G. (1992): Phosphorus sorption by peat and sand amended with iron oxide or steel wool. In: Water Environmental Research 64 (5), pg. 699–705.

Johnson, D. M.; Hokanson, D. R.; Zhang, Q.; Czupinski, K. D.; Tang, J. (2008a): Feasibility of water purification technology in rural areas of developing countries. In: Journal of Environmental Management 88 (3), pg. 416–427.

Johnson, R. L.; Thoms, R. B.; O'Brien Johnson, R.; Krug, T. (2008b): Field Evidence for Flow Reduction through a Zero-Valent Iron Permeable Reactive Barrier. In: Ground Water Monitoring and Remediation 28 (3), pg. 47–55.

Johnson, T. L.; Scherer, M. M.; Tratnyek, P. G. (1996): Kinetics of Halogentated Organic Compound Degradation by Iron Metal. In: Environ. Sci. Technol. 30 (8), S. 2634–2640.

Kabata Pendias, A.; Pendias, H. (2001): Trace Elements in Soil and Plants. 3. Aufl. Boca Raton, Florida: CRC Press.

Karthikeyan, K. G.; Elliot, H.; Cannon, F. (1997): Adsortion and Coprecipitation of Copper with the Hydrous Oxides of Iron and Aluminum. In: Environ. Sci. Technol. 31, pg. 2721–2725.

Kim, H.; Yang, H.; Kim, J. (2014): Standardization of the reducing power of zero-valent iron using iodine. In: Journal of Environmental Science and Health Part A 49, pg. 514–523.

Lackovic, J.; Nickolaidis, N.; Dobbs, G. (2000): Inorganic arsenic removal by zero-valent iron. In: Environmental Engineering Science 17 (1), pg. 29–39.

Leupin, O. X.; Hug, S. J. (2005): Oxidation and removal of arsenic (III) from aerated groundwater by filtration through zero-valent iron. In: Water Research 39 (9), pg. 1729–1740.

Li, S.; Ding, Y.; Wang, W.; Lei, H. (2016): A facile method for determining the Fe(0) content and reactivity of zero valent iron. In: Analytical Methods 8 (6), pg. 1239–1248.

Liou, Y. H.; Lo, S. L.; Lin, C. J.; Kuan, W. H.; Weng, S. C. (2005): Effects of iron surface pretreatment on kinetics of aqueous nitrate reduction. In: Journal of Hazardous Materials 126 (1-3), pg. 189 194.

Makota S., Nde-Tchoupe I.A., Mwakabona H.T., Tepong-Tsindé R., Noubactep C., Nassi A., Njau K.N. (2017): Metallic iron for water treatment: Leaving the valley of confusion. Applied Water Science, doi: 10.1007/s13201-017-0601-x.

Matheson, L. J.; Tratnyek, P. G. (1994): Reductive Dehalogenation of Chlorinated Methanes by Iron Metal. In: Environ. Sci. Technol. 28, pg. 2045–2053.

Miyajima, K. (2012): Optimizing the design of metallic iron filters for water treatment. In: Freiburg Online Geosciences 32.

Momba, M.; Obi, C. L.; Thompson, P. (2009): Survey of disinfection efficiency of small drinking water treatment plants: Challenges facing small water treatment plants in South Africa. In: Water SA 35 (4), pg. 485–494.

Mwakabona, H. T.; Ndé-Tchoupé, A. I.; Njau, K.; Noubactep, C.; Wydra, K. D. (2017): Metallic iron for safe drinking water provision: Considering a lost knowledge. In: Water Research 117, pg. 127 142.

Nair, K. R.; Manji, F.; Gitonga, J. N. (1984): The occurence and distribution of fluoride in groundwaters of Kenya. In: Challenges in African Hydrology and Water Resources IAHS Pub. 144, pg. 75–86.

Naseri, E.; Ndé-Tchoupé, A. I.; Mwakabona, H. T.; Nanseu-Njiki, C. P.; Noubactep, C.; Njau, K.; Wydra, K. D. (2017): Making Fe0-Based Filters a Universal Solution for Safe Drinking Water Provision. In: Sustainability 9 (7), pg. 1224.

National Academy of Sciences (2006): Fluoride in Drinking Water- A Scientific Review of the EPA's Standards. Washington, DC: The National Academic Press.

Ndé-Tchoupé, A. I.; Crane, R. A.; Hezron, T. Mwakabona; Noubactep, C.; Njau, K. (2015): Technologies for decentralized fluoride removal: Testing metallic iron based filters. In: Water Altern 7, pg. 6750–6774.

Ndé-Tchoupé, A. I.; Lufingo, M.; Hu, R.; Gwenzi, W.; Ntwampe, S. K. O.; Noubactep, C.; Njau, K. (2018a): Avoiding the use of exhausted drinking water filters: a filter-clock based on rusting iron. In:Water 10, 591.

Ndé-Tchoupé, A. I.; Makota, S.; Nassi, A.; Hu, R.; Noubactep, C. (2018b): The suitability of pozzolan as admixing aggregate for Fe0-based filters. In: Water 10 (4): 417.

Ngai, T.; Shrestha, R.; Dangol, B.; Maharjan, M.; Murcott, S. (2007): Design for sustainable development Household drinking water for filter for arsenic and pathogen treatment in Nepal.
In: Journal of Environmental Science and Health Part A 42 (12), pg. 1879–1888.

Noubactep, C. (2007): Processes of Contaminant Removal in "Fe0-H2O" Systems Revisited: Importance of Co-Precipitation. In: Open Environmental Sciences 1 (9-13).

Noubactep, C. (2008): A Critical Review on the process of Contaminant Removal in Fe0-H2O Systems. In: Environmental Technology 29 (8).

Noubactep, C. (2009a): Characterizing the discoloration of methylene blue in Fe0/H2O systems. In: Journal of Hazardous Materials 166 (1), pg. 79–87.

Noubactep, C. (2009b): Characterizing the effects of shaking intensity on the kinetics of metallic iron dissolution in EDTA. In: Journal of Hazardous Materials 170(2-3), pg. 1149–1155.

Noubactep, C. (2010a): Characterizing the reactivity of metallic iron in Fe0/EDTA/H20 systems with column experiments. In: Chemical Engineering Journal 162, pg. 656–661.

Noubactep, C. (2010b): Dimensioning metallic iron beds for efficient contaminant removal. In: Chemical Engineering Journal 163 (1), pg. 454–460.

Noubactep, C. (2010c): The fundamental mechanism of aqueous contaminant removal by metallic iron. In: Water SA 36 (5), pg. 663–670.

Noubactep, C. (2010d): The Suitablity of Metallic Iron for Environmental Remediation. In: Environmental Progress and Sustainable Energy 29 (3), pg. 286–291.

Noubactep, C. (2011): Metallic Iron for Safe Drinking Water Production. In: Freiburg Online Geology 27, pg. 1–43. Online verfügbar unter http://tu-freiberg.de/sites/default/files/media/institut fuer geologie-718/pdf/fog_vol_27.pdf.

Noubactep, C. (2015): Metallic iron for environmental remediation: A review of reviews. In: Water Research 85, pg. 114–123.

Noubactep, C. (2016): Designing metallic iron packed beds for water treatment. In: CLEAN- Soil, Water, Air 44, pg. 411–421.

Noubactep C. (2017): Metallic iron for water treatment: Lost science in the West. Bioenergetics 6, 149. doi:10.4172/2167-7662.1000149.

Noubactep, C. (2018): Metallic iron (Fe0) provide possible solution to universal safe drinking water provision. In: J. Water Technol. Treat. Methods 1(1): 102.

Noubactep C. (2018b): Metallic iron for environmental remediation: How experts maintain a comfortable status quo. Fresenius Environmental Bulletin 27, 1379–1393.

Noubactep C. (2018c): The operating mode of Fe0/H2O systems: Hidden truth or repeated nonsense? Fresenius Environmental Bulletin (In press).

Noubactep, C.; Caré, S. (2013): Enhancing the sustainability of household filters by mixing metallic iron with porous materials. In: Chemical Engineering Journal 162 (2), pg. 635–642.

Noubactep, C.; Caré, S.; Btatkeu-K, B. D.; Nanseu-Njiki, C. P. (2012a): Enhancing the Sustainability of Household Fe0/Sand Filters by using Bimetallics and MnO2. In: CLEAN- Soil, Water, Air 40 (1), pg. 100–109.

Noubactep, C.; Caré, S.; Tongue-Kamga, F.; Schöner, A.; Woafo, P. (2010): Extending Service Life of Household Water Filters by Mixing Metallic Iron with Sand. In: CLEAN- Soil, Water, Air 38 (10), pg. 951–959.

Noubactep, C.; Fall, M.; Meinrath, G.; Merkel, B. (2004): A Simple Method to select Zerovalent Iron Materials for Groundwater Remediation. In: in 57th Canadian Geotechnical conference/ 5th Joint CGS/IAH-CNC conference Session 1A, pg. 6–13.

Noubactep, C.; Kurth, A. M.; Sauter, M. (2009a): Evaluation of the effects of shaking intensity on the process of methylene blue discoloration by metallic iron. In: Journal of Hazardous Materials 169 (1-3), pg. 1005–1011.

Noubactep, C.; Licha, T.; Scott, T. B.; Fall, M.; Sauter, M. (2009b): Exploring the influence of operational parameters on the reactivity of elemental iron materials. In: Journal of Hazardous Materials 172 (2-3), pg. 943–951.

Noubactep, C.; Meinrath, G.; Dietrich, P.; Sauter, M.; Merkel, B. J. (2005): Testing the Suitability of Zerovalent Iron Materials for Reactive Walls. In: Environmental Chemistry (2), pg. 71–76.

Noubactep, C.; Schöner, A.; Woafo, P. (2009c): Metallic Iron Filters for Universal Access to Safe Drinking Water. In: CLEAN- Soil, Water, Air 37 (12), pg. 930–937.

Noubactep, C.; Temgoua, E.; Rahman, M. A. (2012b): Designing iron-amended biosand filters for decentralized safe drinking water provision. In: CLEAN- Soil, Water, Air 40, pg. 798–807.

Nowak, B.; Lutzenkirchen, J.; Behra, P.; Sigg, L. (1996): Modeling the Adsorption of Metal-EDTA Complexes onto Oxides. In: Environ. Sci. Technol. 30 (7), pg. 2397–2405.

Peter-Varbanets, M.; Guger, W.; Pronk, W. (2012): Intermittent operation of ultra-low pressure ultrafiltration for decentralized drinking water treatment. In: Water Research 46 (10), pg. 3272 -3282.

Phukam, M. (2015): Characterizing the ion-selective nature of Fe0-based systems using azo dyes: batch and column experiments 42, pg. 1–101. http://tu freiberg.de/sites/default/files/media/institute fuer-geologie 718/pdf/fog_volume_42_final.pdf.

Pierce, E. M.; Wellman, D. M.; Lodge, A. M.; Rodriguez, E. A. (2007): Experimental determination of the dissolution kinetics of zero-valent iron in the presence of organic complexants. In: Environmental Chemistry 4 (4), pg. 260–270.

Piwowarsky, E. (1951): Hochwertiges Gußeisen: Springer Verlag, 1070 pp.

Ponder, S. M.; Darab, J. G.; Mallouk, T. E. (2000): Remediation of Cr(VI) and Pb(II) Aqueous Solutions Using Supported, Nanoscale Zero-valent Iron. In: Environ. Sci. Technol. 24 (12), pg. 2564 2569.

Reardon, E. J. (1995): Anaerobic Corrosion of Granular Iron: Measurement and Interpretation of Hydrogen Evolution Rates. In: Environ. Sci. Technol. 29, pg. 2936–2945.

Reardon, E. J. (2005): Zerovalent Irons: Styles of Corrosion and Inorganic Control on Hydrogen Pressure Buildup. In: Environ. Sci. Technol. 39 (18), pg. 7311–7317.

Reynolds, G. W.; Hoff, J. T.; Gillham, R. W. (1990): Sampling Bias Caused by Materials Used to Monitor Halocarbons in Groundwater. In: Environ. Sci. Technol. 24, pg. 135–142.

Roy, S.; Dass, G. (2013): Fluoride Contamination in Drinking Water-A Review. In: Resources and Environment 3 (3), pg. 53–58.

Sarin, P.; Snoeyink, V. L.; Bebee, J.; Jim, K. K.; Beckett, M. A.; Kriven, W. M.; Clement, J. A. (2004a):Iron release from corroded pipes in drinking water distribution systems: Effect of dissolved oxygen. In: Water Research 38 (5), pg. 1259–1269.

Sarin, P.; Snoeyink, V. L.; Kriven, W. M.; Clement, J. A. (2001): Physico-chemical characteristics of corrosion scales in old iron pipes. In: Water Research 35 (12), pg. 2961–2969.

Sarin, P.; Snoeyink, V. L.; Lytle, D. A.; Kriven, W. M. (2004b): Iron Corrosion Scales: Models for Scale Growth, Iron Release, and Colored Water Formation. In: Journal of Environmental Engineering 130 (4), pg. 364–373.

Saywell, L.G; Cunningham, B. B. (1937): Determination of Iron: Colorimetric o-Phenanthroline Method. In: Ind. Eng. Chem. Anal. Ed 9(2), pg. 67–69.

Schäfer, A. I.; Broekmann, A.; Richards, B. S. (2007): Renewable energy powered membrane technology. 1. Development and characterization of a photovolltaic hybrid membrane system. In: Environ. Sci. Technol. 41, pg. 998–1003.

Scherer, M.; Richter, S.; Valentine, R.; Alvarez, P. (2000): Chemistry and Microbiology of Permeable Reactive Barriers for In Situ Groundwater Clean up. In: Critical Reviews in Microbiology 26 (4), pg. 221–264.

Sikora, E.; Macdonald, D. D. (2000): The Passivity of Iron in the Presence of Ethylenediaminetetraacetic Acid I. General Electrochemical Behavior. In: Journal of the Electrochemical Society 147 (11), pg. 4087–4092.

Sima, L. C.; Elimelech, M. (2013): More than a drop in the bucket: Decentralized membrane-based drinking water refill stations in Southeast Asia. In: Environ. Sci. Technol. 47 (14), pg. 7580 7588.

Slaughter, S. (2010): Improving the sustainability of water treatment systems: Opportunities for innovation. In: Solutions 1, pg. 42–49.

Smith, P. G.; Coakley, P. (1983): A method for determining specific surface area of activated sludge by dye adsorption. In: Water Research 17 (5), pg. 595–598.

Stratmann, M.; Müller, J. (1994): The mechanism of the oxygen reduction on rust-covered metal substances. In: Corrosion Science 36 (2), pg. 327–359.

Teotia, S. P. S.; Teotia, M.; Singh, R. K. (1981): Hydro-Geochemical Aspects of Endemic Skeletal Fluorosis in India- An Epidemiologic Study. In: Fluoride 14 (2), pg. 69–74.

Tepong-Tsinde, R.; Crane, R.; Noubactep, C.; Nassi, A.; Ruppert, H. (2015): Testing Metallic Iron Filtration Systems for Decentralized Water Treatment at Pilot Scale. In: Water 7, pg. 868–897.

Trois, C.; Cibati, A. (2015): South Afrian sands as a low cost alternative solution for arsenic removal from industrial effluents in permeable reactive barriers: Column tests. In: Chemical Engineering Journal 259 (981-989).

Tseng, C. L.; Yang, M. H.; Lin, C. C. (1984): Rapid determination of cobalt-60 in sea water with steel wool adsorption. In: Journal of Radioanalytical and Nuclear Chemistry 85 (4), pg. 253–259.

USAPHC (2011): Filtration in the use of individual water purificaton devices, Technical Information. In: Paper # 31-004-0211.

Vasireddy, D. (2005): Arsenic adsorption onto iron-chitosan composite from drinking water. In: Master Thesis of University of Missouri-Columbia.

Weber, E. J. (1996): Iron-mediated reductive transformations: investigation of reaction mechanism. In: Environ. Sci. Technol. 30, pg. 716–719.

Westerhoff, P.; James, J. (2003): Nitrate removal in zero-valent iron packed columns. In: Water Research 37 (8), pg. 1818–1830.

WHO (2017): Guidelines for Drinking Water Quality. Fourth Edition Incorporating the First Addendum.

You, Y.; Han, J.; Chiu, P. C.; Jin, Y. (2005): Removal and Inactivation of Waterborne Viruses Using Zerovalent Iron. In: Environ. Sci. Technol. 39 (23), pg. 9263–9269.

Zeeck, A.; Fischer, S. C.; Grond, S.; Papastravrou, I. (2003): Chemie für Mediziner. 5. Aufl. München: Urban and Fischer Verlag.

Ziyan, L.; Huang, D.; McDonald, L. M. (2017): Heterogenous selenite reduction by zero-valent iron steel wool. In: Water Science and Technology 75 (3-4), pg. 908–915.

Appendix

Iron dissolution batch experiments in 2mM EDTA solution

App. Table *1*: Experimental data for 0.1 g SW1-SW8 in 50 mL EDTA

Δt	SW1	SW2	SW3	SW4	SW5	SW6	SW7	SW8
(hours)	(mg/L)	(mg/L)	(mg/L)	(mg/L)	(mg/L)	(mg/L)	(mg/L)	(mg/L)
4	10.0	12.0	8.0	12.0	44.0	64.0	78.0	0.0
22	66.0	62.0	46.0	58.0	106.0	108.0	106.0	0.0
48	88.0	76.0	104.0	108.0	78.0	82.0	78.0	0.0
72	110.0	102.0	96.0	128.0	72.0	78.0	68.0	1.1

App. Table *2*: Experimental data for 0.01 g SW1-SW8 in 50 mL EDTA

Δt	SW1	SW2	SW3	SW4	SW5	SW6	SW7	SW8
(h)	(mg/L)	(mg/L)	(mg/L)	(mg/L)	(mg/L)	(mg/L)	(mg/L)	(mg/L)
3.17	7.5	11.5	13.0	10.5	11.5	11.5	11.0	0.0
6.00	28.0	15.0	21.0	20.0	19.0	20.0	18.0	0.0
11.50	30.0	29.0	39.0	35.0	40.0	40.0	34.0	0.0
24.25	54.0	58.0	68.0	63.0	57.0	72.0	60.0	0.0
30.50	54.0	71.0	73.0	71.0	73.0	82.0	73.0	0.0

App. Table *3*: Experimental data for 0.01 g SW1-SW8 in 100 mL EDTA

Δt	SW1	SW2	SW3	SW4	SW5	SW6	SW7	SW8
(h)	(mg/L)	(mg/L)	(mg/L)	(mg/L)	(mg/L)	(mg/L)	(mg/L)	(mg/L)
3.17	5.0	7.5	10.5	7.0	6.0	10.0	8.0	0.0
6.00	6.0	9.0	12.0	9.0	11.0	14.0	11.0	0.0
11.50	13.0	20.0	25.0	17.0	21.0	24.0	21.0	0.0
24.25	31.0	31.0	45.0	35.0	42.0	46.0	40.0	0.0
30.50	36.0	36.0	54.0	42.0	52.0	51.0	49.0	0.0

App. Table *4*: Experimental data for 0.01 g SW9-SW15 and GI in 50 mL EDTA

Δt	SW9	SW10	SW11	SW12	SW13	SW14	SW15	GI
(h)	(mg/L)	(mg/L)	(mg/L)	(mg/L)	(mg/L)	(mg/L)	(mg/L)	(mg/L)
3.17	10.0	16.0	0.0	0.5	0.0	0.0	0.0	0.0

6.00	17.0	23.0	0.0	2.0	0.0	0.0	0.0	0.0
11.50	25.0	37.0	0.0	5.0	4.0	1.0	1.0	1.0
24.25	49.0	64.0	0.0	11.0	6.0	10.0	3.0	1.5
30.50	56.0	75.0	0.0	17.0	20.0	12.0	13.0	2.0

App. Table 5: Experimental data for SW1, SW9, SW5, 0.1g GI, and 0.01g GI in 50 mL EDTA.

time	[Fe] SW1	[Fe] SW9	[Fe] SW5	[Fe] 0.1g GI	[Fe] 0.01g GI
(hours)	(mg/L)	(mg/L)	(mg/L)	(mg/L)	(mg/L)
3.17	18.32	16.90	17.77	8.56	6.33
9.75	35.16	34.65	34.47	14.18	6.87
22.50	64.62	61.20	62.69	25.61	13.69
48.75	92.90	96.62	93.21	39.03	17.24
72.75	102.33	110.912	107.87	49.75	21.58
144.00	(-)	(-)	(-)	89.17	58.50

Iron dissolution column experiments in 2mM EDTA solution

App. Table 6: Iron leaching column experiment with SW6

SW6								
Datum	**Run**	**Dt**	**V**	**Dilution**	**$[Fe]_0$**	**[Fe]**	**m_{Fe}**	**Sm_{Fe}**
	(-)	(days)	(mL)	(-)	(mg/L)	(mg/L)	(mg)	(mg)
20.6.17	1	0	350	20	1.3	26.0	9.10	9.10
22.6.17	2	2	345	20	1.2	24.0	8.28	17.38
23.6.17	3	1	350	20	0.6	12.0	4.20	21.58
17.7.17	4	24	360	20	2.7	54.0	19.44	41.02
21.7.17	5	4	360	10	2.8	28.0	10.08	51.10
23.7.17	6	2	350	10	2.3	23.0	8.05	59.15
25.7.17	7	2	350	10	2.2	22.0	7.70	66.85
27.7.17	8	2	360	10	2.4	24.0	8.64	75.49
31.7.17	9	4	350	10	2.7	27.0	9.45	84.94
1.8.17	10	1	360	10	1.6	16.0	5.76	90.70
2.8.17	11	1	350	10	1.8	18.0	6.30	97.00
3.8.17	12	1	340	10	1.9	19.0	6.46	103.46
4.8.17	13	1	350	10	1.6	16.0	5.60	109.06
7.8.17	14	3	340	10	2.5	25.0	8.50	117.56
8.8.17	15	1	360	10	1.6	16.0	5.76	123.32
9.8.17	16	1	350	10	1.6	16.0	5.60	128.92
11.8.17	17	2	350	10	0.5	5.0	1.75	130.67
14.8.17	18	3	385	10	0.3	3.0	1.16	131.83
15.8.17	19	1	350	10	0.1	1.0	0.35	132.18
16.8.17	20	1	350	10	0.1	1.0	0.35	132.53

17.8.17	21	1	360	10	0.1	1.0	0.36	132.89
18.8.17	22	1	355	10	0.1	1.0	0.36	133.24
21.8.17	23	3	350	10	0.4	4.0	1.40	134.64
22.8.17	24	1	360	5	2.8	14.0	5.04	139.68
24.8.17	25	2	360	5	3.5	17.5	6.30	145.98
25.8.17	26	1	360	5	2.9	14.5	5.22	151.20
28.8.17	27	3	360	5	4.5	22.5	8.10	159.30
29.8.17	28	1	360	5	3.1	15.5	5.58	164.88
30.8.17	29	1	365	5	3.1	15.5	5.66	170.54
31.8.17	30	1	360	5	3.0	15.0	5.40	175.94
1.9.17	31	1	355	5	3.0	15.0	5.33	181.26
4.9.17	32	3	360	5	5.1	25.5	9.18	190.44
5.9.17	33	1	350	5	3.2	16.0	5.60	196.04
6.9.17	34	1	360	5	3.2	16.0	5.76	201.80
8.9.17	35	2	360	5	3.9	19.5	7.02	208.82
11.9.17	36	3	365	5	4.1	20.5	7.48	216.31
12.9.17	37	1	360	5	3.7	18.5	6.66	222.97
13.9.17	38	1	360	5	2.9	14.5	5.22	228.19
15.9.17	39	2	365	5	4.2	21.0	7.67	235.85
18.9.17	40	3	360	5	4.4	22.0	7.92	243.77
19.9.17	41	1	360	5	2.6	13.0	4.68	248.45
20.9.17	42	1	360	5	2.8	14.0	5.04	253.49
21.9.17	43	1	370	5	2.4	12.0	4.44	257.93
23.9.17	44	2	365	5	0.2	1.0	0.37	258.30
25.9.17	45	2	355	5	0.8	4.0	1.42	259.72
26.9.17	46	1	360	5	0.3	1.5	0.54	260.26
27.9.17	47	1	360	5	0.8	4.0	1.44	261.70
2.10.17	48	5	360	5	0.6	3.0	1.08	262.78
9.10.17	49	7	355	5	2.0	10.0	3.55	266.33
10.10.17	50	1	355	5	0.3	1.5	0.53	266.86
11.10.17	51	1	360	5	3.3	16.5	5.94	272.80
12.10.17	52	1	355	5	4.3	21.5	7.63	280.43
13.10.17	53	1	360	5	3.8	19.0	6.84	287.27

App. Table 7: Iron leaching column experiment with SW1

SW1								
Datum	**Run**	**Dt**	**V**	**Dilution**	**$[Fe]_0$**	**[Fe]**	**m_{Fe}**	**Sm_{Fe}**
	(-)	(days)	(mL)	(-)	(mg/L)	(mg/L)	(mg)	(mg)
20.6.17	1	0	340	20	1.5	30.0	10.20	10.20
22.6.17	2	2	350	20	1.3	26.0	9.10	19.30
23.6.17	3	1	350	20	1.5	30.0	10.50	29.80
17.7.17	4	24	360	20	2.7	54.0	19.44	49.24
21.7.17	5	4	350	10	2.9	29.0	10.15	59.39
23.7.17	6	2	350	10	2.3	23.0	8.05	67.44
25.7.17	7	2	350	10	2.2	22.0	7.70	75.14
27.7.17	8	2	350	10	2.3	23.0	8.05	83.19

31.7.17	9	4	350	10	2.4	24.0	8.40	91.59
1.8.17	10	1	350	10	1.4	14.0	4.90	96.49
2.8.17	11	1	350	10	1.7	17.0	5.95	102.44
3.8.17	12	1	345	10	1.7	17.0	5.87	108.31
4.8.17	13	1	350	10	1.3	13.0	4.55	112.86
7.8.17	14	3	340	10	2.5	25.0	8.50	121.36
8.8.17	15	1	350	10	1.2	12.0	4.20	125.56
9.8.17	16	1	385	10	1.4	14.0	5.39	130.95
11.8.17	17	2	350	10	2.2	22.0	7.70	138.65
14.8.17	18	3	385	10	2.2	22.0	8.47	147.12
15.8.17	19	1	360	10	1.2	12.0	4.32	151.44
16.8.17	20	1	360	10	1.4	14.0	5.04	156.48
17.8.17	21	1	350	10	1.3	13.0	4.55	161.03
18.8.17	22	1	350	10	1.2	12.0	4.20	165.23
21.8.17	23	3	350	10	2.2	22.0	7.70	172.93
22.8.17	24	1	350	10	1.2	12.0	4.20	177.13
24.8.17	25	2	360	10	1.8	18.0	6.48	183.61
25.8.17	26	1	360	10	1.6	16.0	5.76	189.37
28.8.17	27	3	350	10	2.6	26.0	9.10	198.47
29.8.17	28	1	350	10	1.3	13.0	4.55	203.02
30.8.17	29	1	360	10	1.4	14.0	5.04	208.06
31.8.17	30	1	350	10	1.1	11.0	3.85	211.91
1.9.17	31	1	350	10	1.6	16.0	5.60	217.51
4.9.17	32	3	350	5	4.8	24.0	8.40	225.91
5.9.17	33	1	350	5	2.9	14.5	5.08	230.98
6.9.17	34	1	385	5	2.5	12.5	4.81	235.79
8.9.17	35	2	360	5	3.4	17.0	6.12	241.91
11.9.17	36	3	350	5	4.7	23.5	8.23	250.14
12.9.17	37	1	350	5	2.8	14.0	4.90	255.04
13.9.17	38	1	345	5	2.8	14.0	4.83	259.87
15.9.17	39	2	350	5	3.3	16.5	5.78	265.64
18.9.17	40	3	360	5	3.6	18.0	6.48	272.12
19.9.17	41	1	350	5	3.9	19.5	6.83	278.95
20.9.17	42	1	350	5	2.8	14.0	4.90	283.85
21.9.17	43	1	350	5	0.3	1.5	0.53	284.37
23.9.17	44	2	350	5	0.1	0.5	0.18	284.55
25.9.17	45	2	350	5	0.1	0.5	0.18	284.72
26.9.17	46	1	350	5	0.2	1.0	0.35	285.07
27.9.17	47	1	350	5	0.2	1.0	0.35	285.42
2.10.17	48	5	365	5	0.2	1.0	0.37	285.79
9.10.17	49	7	350	5	0.2	1.0	0.35	286.14
10.10.17	50	1	350	5	0.1	0.5	0.18	286.31
11.10.17	51	1	350	5	3.0	15.0	5.25	291.56
12.10.17	52	1	360	5	4.5	22.5	8.10	299.66
13.10.17	53	1	350	5	3.8	19.0	6.65	306.31

App. Table 8: Iron leaching column experiment with SW5

SW5								
Datum	**Run**	**Dt**	**V**	**Dilution**	**$[Fe]_0$**	**[Fe]**	**m_{Fe}**	**Sm_{Fe}**
	(-)	(days)	(mL)	(-)	(mg/L)	(mg/L)	(mg)	(mg)
20.6.17	1	0	340	20	1.7	34.0	11.56	11.56
22.6.17	2	2	340	20	1.3	26.0	8.84	20.40
23.6.17	3	1	350	20	1.1	22.0	7.70	28.10
17.7.17	4	24	390	20	2.2	44.0	17.16	45.26
21.7.17	5	4	350	10	2.9	29.0	10.15	55.41
23.7.17	6	2	350	10	2.5	25.0	8.75	64.16
25.7.17	7	2	345	10	2.3	23.0	7.94	72.10
27.7.17	8	2	350	10	2.5	25.0	8.75	80.85
31.7.17	9	4	345	10	2.5	25.0	8.63	89.47
1.8.17	10	1	350	10	1.5	15.0	5.25	94.72
2.8.17	11	1	350	10	1.8	18.0	6.30	101.02
3.8.17	12	1	340	10	1.9	19.0	6.46	107.48
4.8.17	13	1	350	10	1.7	17.0	5.95	113.43
7.8.17	14	3	340	10	2.9	29.0	9.86	123.29
8.8.17	15	1	355	10	1.7	17.0	6.04	129.33
9.8.17	16	1	350	10	1.7	17.0	5.95	135.28
11.8.17	17	2	350	10	2.2	22.0	7.70	142.98
14.8.17	18	3	385	10	2.3	23.0	8.86	151.83
15.8.17	19	1	360	10	1.3	13.0	4.68	156.51
16.8.17	20	1	345	10	1.5	15.0	5.18	161.69
17.8.17	21	1	350	10	1.4	14.0	4.90	166.59
18.8.17	22	1	360	10	1.3	13.0	4.68	171.27
21.8.17	23	3	350	10	2.2	22.0	7.70	178.97
22.8.17	24	1	350	10	1.4	14.0	4.90	183.87
24.8.17	25	2	360	10	2.0	20.0	7.20	191.07
25.8.17	26	1	360	10	1.6	16.0	5.76	196.83
28.8.17	27	3	360	10	2.4	24.0	8.64	205.47
29.8.17	28	1	360	10	1.4	14.0	5.04	210.51
30.8.17	29	1	360	10	1.6	16.0	5.76	216.27
31.8.17	30	1	360	10	1.3	13.0	4.68	220.95
1.9.17	31	1	350	10	1.6	16.0	5.60	226.55
4.9.17	32	3	360	5	4.6	23.0	8.28	234.83
5.9.17	33	1	365	5	2.7	13.5	4.93	239.75
6.9.17	34	1	370	5	2.7	13.5	5.00	244.75
8.9.17	35	2	360	5	3.4	17.0	6.12	250.87
11.9.17	36	3	365	5	4.2	21.0	7.67	258.53
12.9.17	37	1	360	5	2.7	13.5	4.86	263.39
13.9.17	38	1	350	5	2.9	14.5	5.08	268.47
15.9.17	39	2	360	5	3	15.0	5.40	273.87
18.9.17	40	3	360	5	5.4	27.0	9.72	283.59
19.9.17	41	1	355	5	2.6	13.0	4.62	288.20
20.9.17	42	1	360	5	2.7	13.5	4.86	293.06
21.9.17	43	1	350	5	0.4	2.0	0.70	293.76
23.9.17	44	2	365	5	0.2	1.0	0.37	294.13

25.9.17	45	2	360	5	0.2	1.0	0.36	294.49
26.9.17	46	1	360	5	0.1	0.5	0.18	294.67
27.9.17	47	1	360	5	0.2	1.0	0.36	295.03
2.10.17	48	5	365	5	0.2	1.0	0.37	295.39
9.10.17	49	7	350	5	0.1	0.5	0.18	295.57
10.10.17	50	1	360	5	0.2	1.0	0.36	295.93
11.10.17	51	1	360	5	2.9	14.5	5.22	301.15
12.10.17	52	1	380	5	3.7	18.5	7.03	308.18
13.10.17	53	1	360	5	3.2	16.0	5.76	313.94

App. Table 9: Iron leaching column experiment with SW7

SW7								
Datum	**Run**	**Dt**	**V**	**Dilution**	**$[Fe]_0$**	**[Fe]**	**m_{Fe}**	**Sm_{Fe}**
	(-)	(days)	(mL)	(-)	(mg/L)	(mg/L)	(mg)	(mg)
20.6.17	1	0	350	20	2.6	52.0	18.20	18.20
22.6.17	2	2	350	20	2.5	50.0	17.50	35.70
23.6.17	3	1	350	20	1.4	28.0	9.80	45.50
17.7.17	4	24	350	20	2.5	50.0	17.50	63.00
21.7.17	5	4	360	10	3.6	36.0	12.96	75.96
23.7.17	6	2	350	10	2.8	28.0	9.80	85.76
25.7.17	7	2	345	10	2.6	26.0	8.97	94.73
27.7.17	8	2	350	10	2.9	29.0	10.15	104.88
31.7.17	9	4	350	10	2.9	29.0	10.15	115.03
1.8.17	10	1	350	10	1.7	17.0	5.95	120.98
2.8.17	11	1	350	10	2.1	21.0	7.35	128.33
3.8.17	12	1	340	10	2.0	20.0	6.80	135.13
4.8.17	13	1	350	10	1.7	17.0	5.95	141.08
7.8.17	14	3	345	10	2.8	28.0	9.66	150.74
8.8.17	15	1	350	10	1.6	16.0	5.60	156.34
9.8.17	16	1	340	10	1.8	18.0	6.12	162.46
11.8.17	17	2	360	10	2.2	22.0	7.92	170.38
14.8.17	18	3	390	10	2.2	22.0	8.58	178.96
15.8.17	19	1	350	10	1.2	12.0	4.20	183.16
16.8.17	20	1	350	10	1.4	14.0	4.90	188.06
17.8.17	21	1	370	10	1.2	12.0	4.44	192.50
18.8.17	22	1	350	10	1	10.0	3.50	196.00
21.8.17	23	3	350	10	2	20.0	7.00	203.00
22.8.17	24	1	350	10	1.5	15.0	5.25	208.25
24.8.17	25	2	340	10	2.3	23.0	7.82	216.07
25.8.17	26	1	350	10	1.6	16.0	5.60	221.67
28.8.17	27	3	360	10	2.4	24.0	8.64	230.31
29.8.17	28	1	350	10	1.1	11.0	3.85	234.16
30.8.17	29	1	375	10	1.4	14.0	5.25	239.41

31.8.17	30	1	350	10	1.2	12.0	4.20	243.61
1.9.17	31	1	350	10	1.5	15.0	5.25	248.86
4.9.17	32	3	340	5	4.8	24.0	8.16	257.02
5.9.17	33	1	350	5	2.7	13.5	4.73	261.75
6.9.17	34	1	365	5	2.6	13.0	4.75	266.49
8.9.17	35	2	360	5	3.2	16.0	5.76	272.25
11.9.17	36	3	360	5	4.0	20.0	7.20	279.45
12.9.17	37	1	380	5	3.2	16.0	6.08	285.53
13.9.17	38	1	350	5	3.0	15.0	5.25	290.78
15.9.17	39	2	355	5	3.1	15.5	5.50	296.28
18.9.17	40	3	350	5	3.9	19.5	6.83	303.11
19.9.17	41	1	355	5	2.7	13.5	4.79	307.90
20.9.17	42	1	355	5	1.9	9.5	3.37	311.27
21.9.17	43	1	365	5	0.3	1.5	0.55	311.82
23.9.17	44	2	360	5	0.9	4.5	1.62	313.44
25.9.17	45	2	350	5	0.1	0.5	0.18	313.62
26.9.17	46	1	355	5	0.2	1.0	0.36	313.97
27.9.17	47	1	355	5	0.1	0.5	0.18	314.15
2.10.17	48	5	365	5	0.1	0.5	0.18	314.33
9.10.17	49	7	350	5	0.2	1.0	0.35	314.68
10.10.17	50	1	355	5	0.2	1.0	0.36	315.04
11.10.17	51	1	360	5	2.7	13.5	4.86	319.90
12.10.17	52	1	360	5	3.2	16.0	5.76	325.66
13.10.17	53	1	360	5	2.9	14.5	5.22	330.88

App. Table *10*: Iron leaching column experiment with granular iron

granular, iPuTech								
Datum	**Run**	**Dt**	**V**	**Dilution**	**$[Fe]_0$**	**[Fe]**	**m_{Fe}**	**Sm_{Fe}**
	(-)	(days)	(mL)	(-)	(mg/L)	(mg/L)	(mg)	(mg)
20.6.17	1	0	600	20	0.1	2.0	1.20	1.20
22.6.17	2	2	650	20	0.1	2.0	1.30	2.50
23.6.17	3	1	640	20	0.1	2.0	1.28	3.78
17.7.17	4	24	650	20	0.8	16.0	10.40	14.18
21.7.17	5	4	650	10	0.5	5.0	3.25	17.43
23.7.17	6	2	670	10	0.5	5.0	3.35	20.78
25.7.17	7	2	660	10	0.3	3.0	1.98	22.76
27.7.17	8	2	650	10	0.5	5.0	3.25	26.01
31.7.17	9	4	660	10	0.4	4.0	2.64	28.65
1.8.17	10	1	650	10	0.1	1.0	0.65	29.30
2.8.17	11	1	650	10	0.3	3.0	1.95	31.25
3.8.17	12	1	665	10	0.2	2.0	1.33	32.58
4.8.17	13	1	660	10	0.1	1.0	0.66	33.24
7.8.17	14	3	665	10	0.3	3.0	2.00	35.24
8.8.17	15	1	650	10	0.1	1.0	0.65	35.89

9.8.17	16	1	660	10	0.2	2.0	1.32	37.21
11.8.17	17	2	670	10	2.2	22.0	14.74	51.95
14.8.17	18	3	685	10	2.2	22.0	15.07	67.02
15.8.17	19	1	660	10	1.3	13.0	8.58	75.60
16.8.17	20	1	670	10	1.4	14.0	9.38	84.98
17.8.17	21	1	670	10	1.5	15.0	10.05	95.03
18.8.17	22	1	670	10	1.4	14.0	9.38	104.41
21.8.17	23	3	680	10	2.2	22.0	14.96	119.37
22.8.17	24	1	680	10	0.1	1.0	0.68	120.05
24.8.17	25	2	680	10	0.2	2.0	1.36	121.41
25.8.17	26	1	670	10	0.3	3.0	2.01	123.42
28.8.17	27	3	680	10	0.3	3.0	2.04	125.46
29.8.17	28	1	670	10	0.2	2.0	1.34	126.80
30.8.17	29	1	670	10	0.1	1.0	0.67	127.47
31.8.17	30	1	680	10	0.1	1.0	0.68	128.15
1.9.17	31	1	670	10	0.2	2.0	1.34	129.49
4.9.17	32	3	690	5	1.0	5.0	3.45	132.94
5.9.17	33	1	680	5	0.6	3.0	2.04	134.98
6.9.17	34	1	680	5	0.5	2.5	1.70	136.68
8.9.17	35	2	670	5	0.8	4.0	2.68	139.36
11.9.17	36	3	680	5	1.1	5.5	3.74	143.10
12.9.17	37	1	680	5	0.7	3.5	2.38	145.48
13.9.17	38	1	680	5	0.6	3.0	2.04	147.52
15.9.17	39	2	680	5	0.2	1.0	0.68	148.20
18.9.17	40	3	680	5	0.3	1.5	1.02	149.22
19.9.17	41	1	680	5	0.2	1.0	0.68	149.90
20.9.17	42	1	680	5	0.1	0.5	0.34	150.24
21.9.17	43	1	680	5	1.0	5.0	3.40	153.64
23.9.17	44	2	680	5	0.5	2.5	1.70	155.34
25.9.17	45	2	680	5	1.9	9.5	6.46	161.80
26.9.17	46	1	680	5	0.2	1.0	0.68	162.48
27.9.17	47	1	680	5	0.7	3.5	2.38	164.86
2.10.17	48	5	680	5	0.3	1.5	1.02	165.88
9.10.17	49	7	680	5	0.2	1.0	0.68	166.56
10.10.17	50	1	680	5	0.3	1.5	1.02	167.58
11.10.17	51	1	680	5	0.7	3.5	2.38	169.96
12.10.17	52	1	680	5	0.8	4.0	2.72	172.68
13.10.17	53	1	670	5	0.7	3.5	2.35	175.02

Dye discoloration batch experiments (8 weeks)

App. Table *11*: Experimental data for discoloration efficiency of MB after 8 weeks of rotational shaking at 75 rpm.

Sample	$[MB]_1$	$[MB]_2$	$[MB]_3$	$[MB]_2$	delta [MB]	P_1	P_2	P_3	P	deltaP
(-)	(mg/L)	(mg/L)	(mg/L)	(mg/L)	(mg/L)	(%)	(%)	(%)	(%)	(%)
Ref.	10.0	10.0	10.0	10.00	0.00	0.0	0.0	0.0	0.0	0.0
SW1	2.7	2.1	2.8	2.53	0.38	73.0	79.0	72.0	74.7	3.8
SW2	2.4	2.5	2.3	2.40	0.10	76.0	75.0	77.0	76.0	1.0
SW3	2.5	2.4	0.6	1.83	1.07	75.0	76.0	94.0	81.7	10.7
SW4	0.3	2.9	3.2	2.13	1.59	97.0	71.0	68.0	78.7	15.9
SW5	2.3	2.3	2.5	2.37	0.12	77.0	77.0	75.0	76.3	1.2
SW6	2.7	2.2	2.6	2.50	0.26	73.0	78.0	74.0	75.0	2.6
SW7	2.8	2.5	2.6	2.63	0.15	72.0	75.0	74.0	73.7	1.5
SW8	10.0	10.0	10.0	10.00	0.00	0.0	0.0	0.0	0.0	0.0
GI	3.8	3.5	3.6	3.63	0.15	62.0	65.0	64.0	63.7	1.5

App. Table *12*: Experimental data for discoloration efficiency of Orange II after 8 weeks of rotational shaking at 75 rpm.

Sample	$[O\ II]_1$	$[O\ II_2$	$[O\ II]_3$	[O II]	delta [O II]	P_1	P_2	P_3	P	deltaP
(-)	(mg/L)	(mg/L)	(mg/L)	(mg/L)	(mg/L)	(%)	(%)	(%)	(%)	(%)
Ref.	10.0	10.0	10.0	10.00	0.00	0.0	0.0	0.0	0.0	0.0
SW1	1.1	0.5	0.4	0.67	0.38	89.0	95.0	96.0	93.3	3.8
SW2	0.8	0.7	0.5	0.67	0.15	92.0	93.0	95.0	93.3	1.5
SW3	0.4	0.4	0.4	0.40	0.00	96.0	96.0	96.0	96.0	0.0
SW4	0.2	0.3	0.3	0.27	0.06	98.0	97.0	97.0	97.3	0.6
SW5	0.3	0.5	0.2	0.33	0.15	97.0	95.0	98.0	96.7	1.5
SW6	0.4	0.6	1.1	0.70	0.36	96.0	94.0	89.0	93.0	3.6
SW7	0.7	0.9	0.4	0.67	0.25	93.0	91.0	96.0	93.3	2.5
SW8	9.4	9.7	9.6	9.57	0.15	6.0	3.0	4.0	4.3	1.5
GI	1.0	0.6	0.7	0.77	0.21	90.0	94.0	93.0	92.3	2.1

Dye discoloration batch experiments (2 weeks)

App. Table *13*: Experimental data for discoloration efficiency of MB after 2 weeks of rotational shaking at 75 rpm.

Sample	[MB]	delta[MB]	P_1	P_2	P_3	P	deltaP
(-)	(mg/L)	(mg/L)	(%)	(%)	(%)	(%)	(%)
Ref.	10.00	0.56	6.30	-1.92	-4.38	0.00	5.59
SW1	3.28	0.28	63.88	68.76	68.86	67.17	2.84
SW2	1.86	1.30	72.72	96.36	75.05	81.38	13.03
SW3	3.20	0.22	65.50	69.83	68.53	67.95	2.22

SW4	3.06	0.29	70.42	71.65	66.16	69.41	2.88
SW5	1.04	1.22	96.29	75.54	97.03	89.62	12.20
SW6	1.99	1.60	98.46	69.21	72.55	80.07	16.01
SW7	1.86	1.42	97.79	73.79	72.72	81.43	14.17
SW8	10.46	0.26	-1.88	-5.06	-7.00	-4.65	2.58
GI	6.23	0.24	36.86	40.37	35.79	37.67	2.40
SW9	1.25	1.28	93.30	72.80	96.34	87.48	12.81
SW10	0.14	0.02	98.59	98.76	98.40	98.59	0.18
SW11	10.47	0.14	-3.05	-5.82	-5.10	-4.65	1.44
SW12	3.33	1.26	54.06	66.72	79.36	66.71	12.65

App. Table *14*: Experimental data for discoloration efficiency of Orange II after 2 weeks of rotational shaking at 75 rpm.

Sample	**[OII]**	**delta[OII]**	**P_1**	**P_2**	**P_3**	**P**	**deltaP**
(-)	(mg/L)	(mg/L)	(%)	(%)	(%)	(%)	(%)
Ref.	10.00	0.27	3.12	-2.04	-1.07	0.00	2.74
SW1	0.33	0.23	95.77	94.93	99.30	96.66	2.32
SW2	0.30	0.44	99.14	99.86	91.93	96.98	4.38
SW3	-0.06	0.04	100.53	100.30	101.04	100.62	0.38
SW4	0.25	0.13	98.70	96.11	97.83	97.55	1.32
SW5	0.20	0.15	96.58	99.49	98.01	98.03	1.45
SW6	0.22	0.06	97.37	98.45	97.64	97.82	0.56
SW7	0.14	0.07	99.28	97.96	98.61	98.61	0.66
SW8	10.16	0.40	3.00	-4.19	-3.68	-1.63	4.01
GI	4.18	0.16	56.52	59.67	58.28	58.16	1.58
SW9	0.14	0.17	96.71	99.52	99.72	98.65	1.69
SW10	0.31	0.32	93.20	98.34	99.21	96.92	3.25
SW11	10.09	0.48	4.60	-3.44	-3.84	-0.89	4.76
SW12	0.71	0.39	89.11	92.67	96.83	92.87	3.86

Fluoride removal experiments

App. Table *15*: Mass of iron leached in column 1

COLUMN 1	[Fe]	volume	mass Fe	∑ Fe

	(mg/L)	(mL)	(mg)	(mg)
07.08.2017	0	265	0	0
08.08.2017	0.1	270	0.027	0.027
09.08.2017	0.2	275	0.055	0.082
11.08.2017	1.3	300	0.39	0.472
14.08.2017	0	350	0	0.472
15.08.2017	0	245	0	0.472
16.08.2017	0	270	0	0.472
17.08.2017	0	270	0	0.472
18.08.2017	0	295	0	0.472
21.08.2017	0	265	0	0.472
22.08.2017	0.4	325	0.13	0.602
24.08.2017	0.8	335	0.268	0.87
25.08.2017	0.2	335	0.067	0.937
28.08.2017	0	255	0	0.937
29.08.2017	1	335	0.335	1.272
30.08.2017	0.1	305	0.0305	1.3025
31.08.2017	0.5	335	0.1675	1.47
01.09.2017	0.1	325	0.0325	1.5025
04.09.2017	0.3	295	0.0885	1.591
05.09.2017	0.2	345	0.069	1.66
06.09.2017	0.2	290	0.058	1.718
08.09.2017	0.2	335	0.067	1.785
11.09.2017	1.6	285	0.456	2.241
12.09.2017	0.2	330	0.066	2.307
13.09.2017	2.6	345	0.897	3.204
15.09.2017	0	300	0	3.204
18.09.2017	0	275	0	3.204
19.09.2017	0	280	0	3.204
20.09.2017	0	330	0	3.204
26.09.2017	6	235	1.41	4.614
27.09.2017	0	245	0	4.614
02.10.2017	0.6	315	0.189	4.803
06.10.2017	0.5	320	0.16	4.963

App. Table *16*: Mass of iron leached in column 2

COLUMN 2	[Fe]	volume	mass Fe	∑ Fe
	(mg/L)	(mL)	(mg)	(mg)
07.08.2017	0	520	0	0
08.08.2017	2.6	385	1.001	1.001
09.08.2017	0.4	290	0.116	1.117
11.08.2017	1.4	300	0.42	1.537
14.08.2017	0	335	0	1.537
15.08.2017	0	305	0	1.537
16.08.2017	0	305	0	1.537

17.08.2017	0.2	305	0.061	1.598
18.08.2017	0.1	295	0.0295	1.6275
21.08.2017	0	295	0	1.6275
22.08.2017	0.4	330	0.132	1.7595
24.08.2017	0.1	325	0.0325	1.792
25.08.2017	0	325	0	1.792
28.08.2017	0	340	0	1.792
29.08.2017	0.8	330	0.264	2.056
30.08.2017	0	305	0	2.056
31.08.2017	0	315	0	2.056
01.09.2017	0.9	325	0.2925	2.3485
04.09.2017	0	320	0	2.3485
05.09.2017	0	340	0	2.3485
06.09.2017	0.1	310	0.031	2.3795
08.09.2017	0	340	0	2.3795
11.09.2017	0	315	0	2.3795
12.09.2017	0	355	0	2.3795
13.09.2017	0.2	310	0.062	2.4415
15.09.2017	0	310	0	2.4415
18.09.2017	0	300	0	2.4415
19.09.2017	0	325	0	2.4415
20.09.2017	0	250	0	2.4415
26.09.2017	0	285	0	2.4415
27.09.2017	0	295	0	2.4415
02.10.2017	0	310	0	2.4415
06.10.2017	0	305	0	2.4415

App. Table *17*: Mass of iron leached in column 3

COLUMN 3	[Fe]	volume	mass Fe	∑ Fe
	(mg/L)	(mL)	(mg)	(mg)
07.08.2017	0.5	300	0.15	0.15
08.08.2017	0.8	290	0.232	0.382
09.08.2017	1	305	0.305	0.687
11.08.2017	0.4	220	0.088	0.775
14.08.2017	0	310	0	0.775
15.08.2017	0	285	0	0.775
16.08.2017	0	325	0	0.775
17.08.2017	0	320	0	0.775
18.08.2017	0	330	0	0.775
21.08.2017	0	305	0	0.775
22.08.2017	0.4	320	0.128	0.903
24.08.2017	0.4	335	0.134	1.037
25.08.2017	0	340	0	1.037
28.08.2017	0	290	0	1.037
29.08.2017	0	340	0	1.037
30.08.2017	0	285	0	1.037

31.08.2017	0	320	0	1.037
01.09.2017	0	310	0	1.037
04.09.2017	0	310	0	1.037
05.09.2017	0	345	0	1.037
06.09.2017	0	320	0	1.037
08.09.2017	0	350	0	1.037
11.09.2017	0	305	0	1.037
12.09.2017	0.2	330	0.066	1.103
13.09.2017	0.1	300	0.03	1.133
15.09.2017	0	330	0	1.133
18.09.2017	0	300	0	1.133
19.09.2017	0	300	0	1.133
20.09.2017	0	330	0	1.133
26.09.2017	0	215	0	1.133
27.09.2017	0	290	0	1.133
02.10.2017	0	320	0	1.133
06.10.2017	0	330	0	1.133

App. Table *18*: Mass of iron leached in column 4

COLUMN 4	[Fe]	volume	mass Fe	∑ Fe
	(mg/L)	(mL)	(mg)	(mg)
07.08.2017	0.5	605	0.3025	0.3025
08.08.2017	2.5	320	0.8	1.1025
09.08.2017	0.1	295	0.0295	1.132
11.08.2017	1.4	310	0.434	1.566
14.08.2017	0.5	330	0.165	1.731
15.08.2017	0	285	0	1.731
16.08.2017	0	310	0	1.731
17.08.2017	0	295	0	1.731
18.08.2017	0	315	0	1.731
21.08.2017	0	305	0	1.731
22.08.2017	0.4	315	0.126	1.857
24.08.2017	0	330	0	1.857
25.08.2017	0	335	0	1.857
28.08.2017	0	315	0	1.857
29.08.2017	0.5	335	0.1675	2.0245
30.08.2017	0	315	0	2.0245
31.08.2017	0	320	0	2.0245
01.09.2017	0	315	0	2.0245
04.09.2017	0.2	315	0.063	2.0875
05.09.2017	0.1	340	0.034	2.1215
06.09.2017	0	335	0	2.1215
08.09.2017	0.1	350	0.035	2.1565
11.09.2017	0	295	0	2.1565
12.09.2017	0.3	335	0.1005	2.257
13.09.2017	0.2	285	0.057	2.314

15.09.2017	0	300	0	2.314
18.09.2017	0	335	0	2.314
19.09.2017	0	325	0	2.314
20.09.2017	0	320	0	2.314
26.09.2017	0	285	0	2.314
27.09.2017	0	290	0	2.314
02.10.2017	0	285	0	2.314
06.10.2017	0	300	0	2.314

App. Table *19*: Mass of iron leached in column 5

COLUMN 5	[Fe]	volume	mass Fe	∑ Fe
	(mg/L)	(mL)	(mg)	(mg)
07.08.2017	1.4	275	0.385	0.385
08.08.2017	1.4	315	0.441	0.826
09.08.2017	0.9	310	0.279	1.105
11.08.2017	2.5	320	0.8	1.905
14.08.2017	1.3	315	0.4095	2.3145
15.08.2017	0	293	0	2.3145
16.08.2017	0	325	0	2.3145
17.08.2017	0	300	0	2.3145
18.08.2017	0	300	0	2.3145
21.08.2017	0	300	0	2.3145
22.08.2017	0.5	320	0.16	2.4745
24.08.2017	0	325	0	2.4745
25.08.2017	0.1	325	0.0325	2.507
28.08.2017	0	355	0	2.507
29.08.2017	1.1	330	0.363	2.87
30.08.2017	0.1	305	0.0305	2.9005
31.08.2017	0.7	315	0.2205	3.121
01.09.2017	0.2	295	0.059	3.18
04.09.2017	0.1	325	0.0325	3.2125
05.09.2017	0.2	335	0.067	3.2795
06.09.2017	0.1	305	0.0305	3.31
08.09.2017	0.6	330	0.198	3.508
11.09.2017	0	310	0	3.508
12.09.2017	0.2	360	0.072	3.58
13.09.2017	0.5	300	0.15	3.73
15.09.2017	0.4	300	0.12	3.85
18.09.2017	0	335	0	3.85
19.09.2017	0	310	0	3.85
20.09.2017	0	320	0	3.85
26.09.2017	0	285	0	3.85
27.09.2017	0	290	0	3.85
02.10.2017	0	280	0	3.85

06.10.17	0.3	290	0.087	3.937

App. Table *20*: Overview of fluoride concentration measured in column experiments

Leaching event	**Column 1**	**Column 2**	**Column 3**	**Column 4**	**Column 5**
(-)	F- (mg/L)	F- (mg/L)	F- (mg/L)	F- (mg/L)	F- (mg/L)
1	7.4	10.5	8.1	10.5	13.1
2	19.5	19.5	20.4	21.3	22.2
3	22.2	22.2	23.2	25.3	25.3
4	22.2	23.2	23.2	25.3	25.3
5	20.4	22.2	22.2	25.3	25.3
6	20.4	21.3	22.2	22.2	23.2
7	20.4	21.3	21.3	22.2	23.2
8	19.5	20.4	21.3	22.2	22.2
9	20.4	21.3	21.3	22.2	22.2
10	19.5	21.3	21.3	23.2	23.2
11	20.4	21.3	22.2	23.2	23.2
12	21.3	22.2	23.2	23.2	24.3
13	21.3	22.2	22.2	24.3	24.3
14	21.3	21.3	22.2	23.2	23.2
15	21.3	22.2	22.2	23.2	24.3
16	21.3	22.2	22.2	23.2	23.2
17	21.3	22.2	22.2	23.2	24.3
18	19.5	21.3	22.2	23.2	23.2
19	20.4	21.3	22.2	23.2	23.2
20	19.5	21.3	22.2	23.2	24.3
21	23.2	24.3	25.3	25.3	25.3
22	23.2	22.2	24.3	25.3	25.3
23	23.2	23.2	24.3	25.3	25.3
24	22.2	24.3	20.4	25.3	24.3
25	20.1	19.3	20.1	22.7	20.9
26	14.8	15.4	15.4	15.4	14.8
27	18.9	16.1	18.9	14.8	19.7
28	17.5	16.1	19.7	19.7	17.5
29	20.6	19.7	21.4	24.2	22.3
30	22.7	22.7	22.7	22.7	22.7
31	22.7	22.7	22.7	22.7	23.6
32	20.9	20.9	20.9	20.9	20.9
33	23.6	23.6	23.6	23.6	22.7
34	23.6	22.7	23.6	22.7	23.6
35	23.6	24.6	22.7	21.8	21.8
36	21.8	20.9	20.9	20.9	22.7
37	19.9	19.9	20.8	20.8	20.8
38	20.4	20.4	19.6	19.6	19.6
39	22.2	22.2	22.2	22.2	22.2
40	14.4	15.0	15.0	15.0	15.0
41	19.4	19.4	19.4	20.3	20.3

42	19.4	20.3	20.3	20.3	21.1
43	20.3	20.3	20.3	21.1	21.1
44	21.1	20.3	21.1	21.1	22.0